

X RAYS FROM MUON, PION, KAON, AND SIGMA-MINUS CAPTURE
IN THE LIGHT ELEMENTS

S. Berezin, G. Burleson, D. Eartly, A. Roberts
and T. O. White

December 1969



X RAYS FROM MUON, PION, KAON, AND SIGMA-MINUS CAPTURE
IN THE LIGHT ELEMENTS*

S. Berezin

Argonne National Laboratory, Argonne, Illinois, 60439

G. Burleson

Northwestern University, Evanston, Illinois, 60202

D. Eartly[†]

Argonne National Laboratory, Argonne, Illinois, 60439

and

The University of Chicago, Chicago, Illinois, 60637

and

A. Roberts and T. O. White

National Accelerator Laboratory, Batavia, Illinois, 60510

December 1969

ABSTRACT

A search for x rays from the capture of kaons in helium has disclosed neither K- nor L-series radiation; the upper limit of the x-ray yield is in the range 7-10 percent. This contradicts results of an earlier measurement but is in better judgment with related data on kaon-helium scattering. In the same experimental arrangement, the yields of pionic and muonic x rays in helium were also measured. We find anomalously low yields, accompanied by intensity distributions of the K-series members in disagreement with the

* This work was performed under the auspices of the U. S. Atomic Energy Commission.

[†] ANL-AMU Predoctoral Fellow. Now at National Accelerator Laboratory.

conventional cascade picture of a predominantly circular set of orbits. Monte Carlo cascade calculations could not duplicate the observed results unless weak Stark mixing, in the form of "sliding transitions" ($n, \ell \rightarrow n, \ell \pm 1$) was added. Agreement with observation was achieved in muonic, pionic, and kaonic atoms with a single value for the parameter describing the strength of the Stark mixing. Yields and energies of kaonic x rays in other light elements, Li, Be, and C, were also measured. Yields of x rays from muonic and pionic capture in these elements were remeasured also, and cascade calculations like those for helium repeated. In these elements the addition of Stark mixing is not needed to achieve agreement with experiment. In the pionic atoms 2p-state absorption rates, and in kaonic atoms 3d-state absorption rates for He, Li, Be, and C can be derived from the experimental data and compared with theoretical values, with good agreement. In addition to the identifiable kaonic transition lines also observed by Wiegand and Mack, additional lines not ascribable to kaonic atoms were found in all three elements. After careful consideration of possible origins of these lines, we ascribe the two lithium lines to M_{α} and M_{β} , and the Be line to M_{α} transitions in sigma-hyperonic atoms. Such atoms are formed if Σ^{-} hyperons from kaon capture (whose abundance is about 15%) are slowed down and stopped in the target. The observed yields and energies are consistent with this interpretation, and with no other

we have been able to invent. A line in C, however, cannot be ascribed either to kaonic or sigma atoms, and appears to be a pionic L_{α} . Why such a line appears only in C is not understood.

I. INTRODUCTION

The primary motivation of the work to be described here was the discrepancy between two sets of experiments on the interaction of slow kaons in helium. The experiment of Burleson et al.¹ on the yield and energies of the K_{α} and L_{α} x rays from the kaonic helium atom indicated an interaction between the kaon and the alpha particle which was not only too weak to accord with current concepts of the kaon-nucleon interaction, but actually was in contradiction with experimental data on kaon-helium scattering.^{2, 3}

Our repetition of the kaonic helium x-ray measurements led to results⁴ at variance with the earlier ones, but in agreement with expectations from kaon-helium scattering and with theoretical models. We found no appreciable K- or L-series x-ray yield, rather than the large yield values reported before. In order to verify these null results, we were led to examine the x-ray yield from muon and pion capture in helium, and the x rays emitted after muon, pion, and kaon capture in other light nuclei. These have resulted in interesting new physics. The absolute yields of muonic and pionic x rays in helium had not been previously measured, and were unexpectedly low. To understand this, we carried out Monte Carlo calculations on the cascade process in the $(\text{He-M})^+$ mesonic ion, a hydrogen-like structure. We found that the results could not be explained without introducing

transitions due to collisions. Collisions produce mixing of angular momentum states in a hydrogen-like atom, by introducing a non-central field, first described as molecular binding by Roberts⁵ and later as Stark transitions by Day, Sucher, and Snow,⁶ who also made quantitative calculations.

The capture of pions and muons in Li, Be, and C allowed remeasurement of the yields and intensity distributions of the K and L series x rays in these elements. The anomalies found in helium were absent, and the cascade is explicable without the introduction of Stark mixing. The 2p-capture rates in pionic atoms have been inferred from the cascade calculations.

II. EXPERIMENTAL SETUP

The experiments were carried out with a proportional counter spectrometer at the Zero Gradient Synchrotron at the Argonne National Laboratory.

A. Beam Design

We used a 16-meter-long, unseparated, two-stage, low-momentum beam with large phase-space acceptance, produced at 0° from a target at the second focus F_2 of the external proton beam (EPB-1) from the Argonne ZGS. A study of K^- stopping efficiency, taking into account production cross sections, decay in flight, and interactions and scattering losses in the moderator, established a broad optimum in the number of stopping kaons at a beam momentum of 800-900 MeV/c.

The calculated optimum for stopping pions and muons was about 300 MeV/c. However, excessive electron contamination and other technical problems led to the choice of 500 MeV/c as the beam momentum to be used.

Figure 1a shows a simplified layout of the beam, including the counters, moderator, target, and shielding.

B. Particle Selection and Detection

Kaon Selection. The selection of a practically pure (>99.5%) signal was achieved with a time-of-flight telescope $C_1 . C_2$ of two liquid Fitch-type inverse threshold Cerenkov counters located at the first and second foci of the beam. A complete description of the counters and their performance has been published.⁷

Pion, Muon Selection. To select the pions or muons in the 500 MeV/c beam, a high-pressure gas-filled (Freon 13) threshold Cerenkov counter C_G replaced C_2 , as in Fig. 1b. It was used in coincidence for muons and in anticoincidence for pions, with a scintillation counter telescope $S_1 . S_2$. The gas counter detected only the muons.

dE/dx Counter. An additional 8.9 cm diameter, 0.63 cm thick dE/dx scintillator S_3 identified slow particles coming out of the moderator. For kaons, a single-channel analyzer on the pulse output was set to detect 4x minimum ionizing particles, corresponding to the average pulse height of kaons stopping in the target. In the K^- beam, pions coming out of

the moderator at ≈ 560 MeV/c were minimum ionizing and thus rejected. The dE/dx criterion provided an additional stopping K/π selection factor greater than 5.

For stopping pions and muons, the dE/dx threshold was reduced to $2\times$ minimum ionizing. The counter was calibrated with protons in a positive beam.

Proportional Counters. The hodoscope used for x-ray detection consisted of four pairs of 0.010 in. Be window proportional counters.⁸ Each counter was 5cm \times 5cm \times 51 cm, and was filled with xenon at 2 atmospheres absolute pressure.

To stop an appreciable fraction of the K^- beam in helium, a 30.5cm long liquid helium target was used. This target length in turn dictated the use of large area detectors to achieve a reasonable solid angle, thus excluding the use of solid-state detectors. The proportional counter hodoscope subtended 0.4 sr at the target, was outside the beam, and had a high detection efficiency for 5-50 keV x rays.

Behind each pair of counters (IJ) an overlapping anti-coincidence scintillation counter AC_{IJ} was used to prevent the analysis of pulses resulting from in-time charged particles traversing the proportional counters, as described below.

C. Triggering Logic

The stopping K^- trigger (\equiv KSTOP) consisted of a C_1, C_2 Cerenkov telescope coincidence with the proper K^- time-of-flight delay (\equiv TOF), in coincidence with the dE/dx counter after the moderator, and in anticoincidence with a downstream

scintillator ACDS behind the targets (Fig. 1a); i.e., $KSTOP = TOF \cdot dE/dx \cdot \overline{ACDS}$. For muons and pions the TOF telescope was replaced by the scintillation counter telescope $S_1 \cdot S_2$, in coincidence with the threshold gas Cerenkov counter C_G for muons ($TOF = S_1 \cdot S_2 \cdot C_G$); and in anticoincidence ($TOF = S_1 \cdot S_2 \cdot \overline{C_G}$) for pions (Fig. 1b).

After forming the KSTOP trigger, the logic generated slow gates from $KSTOP \cdot AC_{IJ}$ for each proportional counter bank.

The data were accumulated in two TMC 1024-channel analyzers, one for data and the other for out-of-time background. The analyzers were divided into four 256-channel quadrants, and the data from each of the four pairs of proportional counters were routed to the appropriate quadrant by tagging signals. Final summing of the data was accomplished by a supplementary computer program. The gains of the two counters of each pair were matched by adjusting the high voltage.

Signal Processing. Each of the four channels of the pulse spectrometer contained a low-noise preamplifier⁹ fed to a direct-coupled low-noise linear pulse amplifier¹⁰ with fixed unipolar (negative) RC integrating and differentiating time constants. The amplifier contained a pole-zero (damping) circuit to reduce spectral distortion due to pulse overshoots and a baseline-restoring circuit to prevent baseline shift with high counting rate. Continuous gain controls allowed a matching of the gains in all four channels. The buffered out-

puts passed to a delay line in the linear gate and to a linear pulse selector which provided a gating signal (control) to the linear gate. Figure 2 shows the signal-processing system used.

The linear pulse selector¹¹ (LPS) is a single-channel analyzer with an additional baseline discriminator to reduce pulse-tail pileup distortion, by requiring a given input pulse to start within +75 mV from the baseline (+0mV). It also contains a pulse-shape discriminator circuit which reduces spectral distortion due to leading-edge pile-up and defective (i.e., oddly shaped) pulses from various backgrounds. Selection is made through zero-crossing detection of the differentiated input pulse. An external direct-coupled gate allowed an enabling or disabling each channel by external logic (KSTOP . \overline{AC}_{IJ} gates). The LPS also contains a strobed coincidence circuit which was used to generate an out-of-time tag (routing) gate for an input of the delayed KSTOP . \overline{AC}_{IJ} slow gate.

The walk-free LPS output provided a gate signal, which in coincidence with the parallel delayed output from the linear pulse amplifier, enabled the linear gate.

The linear gate¹² established proper pulse shaping and final baseline restoration of the analogue pulse for analogue-to-digital conversion and storage.

The four channels were finally merged in a linear mixer in conjunction with an anticoincidence gate which insured that

only one pulse (one channel) entered the mixer, and thus the ADC. By storing the channels independently, the behavior of each channel could be monitored.

D. Targets

The liquid helium target was specially constructed to transmit low-energy x rays.¹³ It was 15.3 cm in diameter, 30.5 cm long, with mylar walls only 0.05 mm thick where the x rays emerged. A beryllium foil heat shield and aluminized mylar outer window minimized the x-ray absorption. A thin window at the bottom allowed an external x-ray source to be used to check the target x-ray transmission.

The solid targets were in the form of rectangular blocks suspended at a shallow angle (about 20°) with respect to the incident beam, thus maximizing the stopping power while minimizing absorption of transversely emerging x rays. Target dimensions were 42.0 cm x 15.5 cm x 1.90 cm (Li); 38.6 cm x 15.3 cm x 2.54 cm (C); 45.5 cm x 15.3 cm x 2.54 cm (Be), with projected (beam direction) thicknesses of 14.10 g/cm² (C); 12.82 g/cm² (Be); 3.39 g/cm² (Li).

III. TESTING AND CALIBRATION

A. Counting Rate Losses

The background in the proportional counters included a wide variety of pulse amplitudes, rise and decay times, and shapes. The overshoots caused by the different pulses, especially those saturating the amplifiers, varied widely. As

the pole-zero damping circuit compensation covered only the normal unsaturated range of pulse heights and shapes, the overshoot could not always be removed. As a consequence, counting losses due to baseline discrimination against pulse-tail (overshoot) pileup occurred. This effect was entirely dominated by large background pulses saturating the amplifier.

To insure that the counting loss was not sensitive to the spectrum of saturated pulses, rate loss tests were conducted both in the beam and with an artificial, induced γ -ray background. The good agreement of the two results assured this independence.

The counting rate losses were about 20 percent at a total singles counting rate per channel (two counters) of 7 KHz. Most of the data were taken at counting rates of 6 KHz or less.

B. Resolving Time of the Proportional Counters

Because of the low electron drift velocity in the outer low-field regions of the xenon proportional counters, a significant time delay of the output pulses occurred for low-energy x rays¹⁴ which are absorbed near the counter window.

To make precise measurements of this delay, gamma-x-ray delayed coincidence measurements were made with weak (0.1 μ c) electron-capture sources Co⁵⁷, Zn⁶⁵, Cd¹⁰⁹. This was done by replacing the KSTOP signal with the output of a NaI γ -ray detector placed in close proximity to the proportional counters.

Measurements were made for different locations on the counters. In addition, tests were made with background added. The results indicated that all counters were similar, the delays were uniform over the window area, and the delay was independent of rate. Figure 3 shows a plot of the variation of counter efficiency with delay, for several different energies of x rays.

This property of the counters made it possible to search for low-energy x rays by varying the coincidence gate-length, a fact which we utilized in looking for the L-series from kaon capture in helium.

C. Linearity and Stability

The pulse spectrometer linearity was established by using an amplitude-stable mercury exponential pulse generator fed into the preamplifiers. The spectrometer was found to be linear with $\pm 1/2\%$ in the ADC range used to collect data spectra.

The variations of amplifier gain K and spectrometer baseline B_0 with rate were found to be less than $\pm 1\%$ ($\delta K/K$) and \pm channel (δB_0), respectively for counting rates from 1 KHz to 40 KHz. Both a variable frequency pulse generator and external x-ray sources were used to establish the rate.

Once the spectrometer system had been brought to equilibrium, it maintained excellent long term stability.

D. Detection Efficiency and Resolution

Counter Efficiencies. The intrinsic efficiency of the

proportional counters as a function of energy was established with the use of standard x-ray sources in a known and constant geometry. The resolution as a function of energy was likewise determined using these sources.

Stopping Distributions. Because of the large size of the targets and proportional counters, the net detection efficiency depended on the distribution of stopping particles over the targets. To determine this distribution for the solid targets, a small scintillation counter S_5 was used in coincidence with the particle stop signal ($S_5 \cdot M_{STOP}$) to generate a grid measurement of the stopping density $M_{STOP}(X)$ over the target face.

With the given target configuration, the muon and pion stopping distributions for the helium target were uniform because of the large divergence (due to scattering) of the stopping beams. For kaons, the stopping beam was more concentrated in a forward cone, but the stopping was again approximately uniform in helium. To establish this, a mock target was made up of a series of incremental absorbers: thin lucite discs spaced with styrofoam to give the same mean density as liquid helium. Using a dE/dx scintillator probe with the exact cross section of the target, measurements of the differential absorption along the target were made. These established the uniformity of stopping for kaons.

E. Geometrical Efficiency

For each target, the spectrometer detection efficiency

$\epsilon_D(E_\gamma)$ was determined with a Monte Carlo program. In this program, the target and spectrometer coordinates were specified, and x-ray emission points were generated in the targets according to the appropriate particle stopping distribution. The x rays were emitted isotropically.

If the given x-ray path intersected one of the counters, its path length in the target was found. Then, given a series of energies, corresponding target absorption coefficients, and counter efficiencies, the probability of detection was determined. Thus, the programs yielded detector solid angle and the energy-dependent detection efficiency $\epsilon_D(E_\gamma)$ averaged over the targets.

F. Yield Determinations: Stopping Measurements

Muons. Recorded data included S_1S_2 (See Fig. 1b) giving the total secondary beam flux, $N_\mu \equiv S_1S_2 \cdot C_G \cdot dE/dx$, the muon flux through the moderator, and $\mu_{STOP} = N_\mu \cdot \overline{ACDS}$, the apparent number of muons stopped. The actual number of muons removed by the target was determined from the range curves for N_μ/S_1S_2 and μ_{STOP}/S_1S_2 vs moderator thickness L_D of copper, for the targets in and out. These range curves indicated, as expected, a large range straggling in the muon stopping in Cu (mean range 250 g/cm^2).

The difference spectrum μ_{STOP}/N_μ (Tgt) - μ_{STOP}/N_μ (no Tgt) yields the muon attenuation due to the target, which is due both to stopping and scattering out.

To correct the muon stopping measurements for scattering,

two procedures were considered. First, the difference spectrum in the scattering region was linearly extrapolated under the stopping region. As a better estimate of the scattering, the muon no-target range curve was used by normalizing it to the transition region between scattering (degrader length $L_D \ll \text{muon range } R_\mu^O$) and stopping ($L_D \approx R_\mu^O$). While the scattering correction for the Be target was small (8%), the corrections for the He, Li targets were large (30%), and the uncertainty in this correction constitutes a major part of the final yield errors.

Pions. For pions $N_\pi \equiv S_1 S_2 \cdot \bar{C}_G \cdot dE/dx$ gave the pion flux through the moderator: $\pi_{STOP} \equiv N_\pi \cdot \overline{ACDS}$ gave the number of pions apparently stopped.

The pion integral and differential range curves indicated a much smaller straggling in the pion stopping range R_π^O (220 g/cm² of Cu). Again, the difference spectrum $\pi_{STOP}/N_\pi (\text{Tgt}) - \pi_{STOP}/N_\pi (\text{no Tgt})$ yielded the pion stopping rate (including scattering).

In the case of the pions, which had a better defined range than muons, the scattering corrections were typically only 10%.

Kaons. For kaons, $N_K \equiv KTOF \cdot dE/dx$ gave the kaon flux through the moderator, and $K_{STOP} \equiv N_K \cdot \overline{ACDS}$ gave the number of stopping kaons. Range curves K_{STOP}/N_K were taken with the targets in and out. The difference spectrum $(K_{STOP}/N_K)_{Tgt} - (K_{STOP}/N_K)_{No Tgt}$ determined the kaon stopping rate. The same procedure for establishing scattering

corrections was followed. Because of the well-defined kaon range R_K^O (217 g/cm² Cu) and small straggling, these corrections were typically 5% in Be, C and 10% in He, Li.

To check the values of K_{STOP}/N_K obtained for the helium target, a scintillator E_{TOT} equivalent to the helium target was used to form "KS" = $K_{STOP} \cdot E_{TOT}$, a kaon-stopping-in-helium signal. With this "KS", a range curve was taken. To extract the stopping, the same procedure used to make scattering and in-flight interaction corrections was followed, with a result in good agreement with that of the earlier procedure.

The yield errors quoted result from adding in quadrature the statistical error in difference spectrum count, zero error and errors in stopping detection efficiency, counting loss and gate width corrections. The dominant errors were the stopping fraction and statistical errors.

G. Escape Peak Measurements

For x-ray energies above the xenon K-absorption edge (at 34.6 keV), escape-peak efficiencies had to be determined in order to establish the correct detection efficiency in the total absorption x-ray peak. Escape-peak yield measurements were made with standard Gd^{153} (40 keV) and Am^{241} (60 keV) sources. These results were cross-checked against escape peaks for the π -Be K_β and π -Be K_α x rays. The agreement indicated that the escape corrections were known to 5-10%.

IV. PROCEDURE AND RESULTS

A. Procedures

Once the conditions for a given data run were established, a calibration run (Fe^{55} and Cd^{109}) in the beam spill was made under running conditions by producing an artificial K_{STOP} signal with a beam-gated signal generator. The singles counting rates of the proportional counters in all calibration runs were within $\pm 10\%$ of the data run rates. Thus the calibration spectrum included any gating, beam spill, background, and rate effects. At various times, this spectrum was cross checked against those of Co^{57} , Cs^{137} , and Am^{241} so that the over-all linearity of the system under these conditions could be established. Calibration runs were interspersed frequently with data runs. Periodic x-ray transmission tests of the liquid He target were made, using a Fe^{55} source.

Data Reduction. Data stored in the 1024-channel analyzers were read out on punched paper tape, transferred to magnetic tape, and run through two data-reduction and spectrum-fitting computer programs. The first of these, HERMES, combined the data, made plots, located peaks in calibration runs, normalized the calibration and data runs, and produced summary data tapes for use by APOLLO, which found peak centroids, made fits to single or multiple peaks, and determined energies, widths, errors, etc.

B. Results: Helium

Muons. An example of the muon difference spectra (in He) is given in Fig. 4. All the muon results are given in Table I. To account for the line-broadening effect of the K_{β} and K_{γ} components, the K-series x-ray energies and intensities were determined by computer multiple-gaussian peak fits. The ratio of K_{α} to the sum of all K-series intensities $K_{\alpha}/\Sigma K_J$ was corrected for relative detection efficiency of each line. For He, the best fits required a small ($\approx 5\%$) K_{γ} component, and the quoted $K_{\beta\gamma}$ energy includes the K_{γ} effects.

Pions. An example of the pion difference spectrum (in He) is given in Fig. 5. Since the spectrum contains muon contamination, multipeak fitting procedures were used. By including the muon lines in the fits, adequate yield determinations and proper energy fits were obtained. All the pion results are given in Table II.

Kaons. A major portion of the running time was devoted to the kaon-He study, with a total of 1.25×10^6 kaons stopped in He. Because of the absence of any x rays, the study included a variety of running conditions. In-time data and out-of-time (random background) spectra were taken with both a short gate (2.5 μ sec) which excluded most of the L_{α} x rays (6.5 keV), and a long coincidence gate ($\geq 4.0\mu$ sec) which admitted most of the L_{α} x rays (See Fig. 3). Both data sets would include all the K-series x rays. Empty target (both in- and out-of-time) backgrounds were also taken with these two gating conditions. Finally, long-gate runs on a dummy He absorptive target, (He

replaced by an equivalent mass and average density styrofoam-lucite sandwich) which allowed no low-energy x rays to emerge, were taken in order to establish whether the spectrometer had detected low energy x-ray signals from He.

Figure 6 illustrates the total data and out-of-time (background) spectra representing 1.25×10^6 kaons stopped in helium. A difference spectrum (target full minus target empty) is shown in Fig. 7. For a 50% K_α yield (34.9 keV) there should be 10^4 x rays in the line.

As there is no evidence for the K-series lines, upper limits to the yields were established. Table III gives the yield limits on the K-series x rays calculated according to a set of varying assumptions. These are:

1. K_α line:
 - a. An unshifted line (corresponding to a K^- - He zero scattering length), with instrumental width only; or
 - b. A shifted line (± 2 keV) with a corresponding 2 keV broadening;
- or, 2. The same conditions as 1, for K_β .

The kaon-helium scattering data of Block et al.,³ yields an s-wave phase shift that predicts a large displacement and broadening of the $1s$ -state; from their values the K_α line would occur at 41.0 keV, with a width of 6.7 keV. Limits of observation are quoted in Table III for such a line also.

The search for L-series x rays also required a detailed analysis of the x-ray data. For the data consisting of ten

independent spectra, there is a set of consistency relations between all the difference spectra combinations which can be formed, which establishes the various signal components present in the spectra.

As the complete analysis is complicated, only the essential results will be given. Figure 8 illustrates the difference spectrum of the 4 μ sec He data and 4 μ sec dummy He data, which established the existence of low-energy signals in the data. The difference spectrum of the 4 μ sec and 2.5 μ sec data (the latter excludes low energy in-time signals) indicated the presence of in-time He and/or target signals, while the difference spectrum of the 4 μ sec data and empty-target background indicated no evidence of L x rays; i.e., in-time He signal. The difference spectrum of the 4 μ sec empty-target (in-time) and the 2.5 μ sec empty-target (in-time) indicated there may be a low energy in-time signal from the empty target, equivalent to that of the 4 μ sec minus 2.5 μ sec He data difference spectrum. Thus the in-time signal is consistent with that from the target alone, i.e., there is no He in-time signal.

The difference spectrum of the 4 μ sec helium out-of-time and empty-target out-of-time backgrounds indicated that there is also an out-of-time low-energy He signal. The difference spectra of the 2.5 μ sec He data and empty-target in-time background vs the 4 μ sec He data and empty-target in-time background indicated that the low-energy He signal in the 4 μ sec data is comparable to that in the 2.5 μ sec He data, again implying that

there is only an out-of-time component, since the latter excluded in-time signals.

Figure 9 shows the difference spectrum of the 4 μ sec data and out-of-time background; again, there is no evidence for a He in-time signal. Finally, Fig. 10 illustrates the difference spectrum which contains only the low-energy He in-time signal. It is from these spectra that the L-series x-ray limits are determined. The results are given in Table IV. A 50% L $_{\alpha}$ yield would correspond to 1.25×10^3 x rays.

In addition, the total kaon-He data and total 4 μ sec kaon-He data spectra were fitted with second order polynomials. Except for the Xe K $_{\alpha}$ x ray there was no statistical evidence for any superposed line structure. Furthermore, using these data spectra and the corresponding out-of-time background spectra, a maximum likelihood search indicated an optimum fit for a zero signal level.

C. Results: - Other Elements

Muon X-Rays. The muon K-series x-ray results in Li and Be, and L-series results in Be and C are given in Table I. Since the μ^{-} -Be K $_{\beta}$ x ray generated a xenon K $_{\alpha}$ escape peak at 9.9 keV, the weaker overlapping μ^{-} -Be L $_{\beta}$ x-ray could not be directly determined. To insure that the L $_{\alpha}$ peak did not include any escape x rays, the L $_{\alpha}$ yield was determined from the difference spectrum of the long (4 μ sec) and the short (2.5 μ sec) coincidence gate data. The short-gate data excludes most of the low-energy (non-escape) structure. Subtracting the short

coincidence gate data removed the low-energy escape peaks which appeared in both spectra and left only the true low-energy in-time x-ray structure. To establish the L-series yield, a 0.15 L_{β} yield was assumed.

Pion X Rays. The K- and L-series x-ray results are given in Table II. Using the muon x rays and standard x-ray sources to establish instrumental line width as a function of energy, pion K x ray natural line width measurements were made.

Kaon X Rays. The L- and M-series x-ray yield results in Li, Be, and C are given in Table V. Energy and line width measurements are included.

V. MESONIC ATOMS: THE DE-EXCITATION PROCESS

The initial formation of a highly excited state (large principal quantum number n) of the bound meson-nucleus system occurs through the replacement (via the Auger effect) of an atomic electron by a meson. The mesonic history in the outermost levels outside the electronic K-shell is unclear; we will mainly concern ourselves with those levels in which the meson is clearly associated with only a single nucleus. Interactions of the mesonic atom with other atoms will be treated as collisions.

A distinction between hydrogen and helium on the one hand, and heavier elements on the other, is made necessary by the nature of the de-excitation cascade. In hydrogen, the meson-nucleus system is neutral; it is physically a hydrogen

atom. In isolation, it would lose energy, if in an excited state, by radiation only, a very slow process for highly excited states. The major energy losses and de-excitation therefore occur in collisions. A similar process occurs in helium; both electrons are rapidly ejected by the Auger effect, leaving a residual alpha-mesonic ion $(\text{He-M})^+$, which can lose energy only by radiation or by collision, specifically in inelastic collisions of the second kind. Direct transfer of energy from the mesonic atom to one of the electrons in the struck atom occurs via the external Auger effect. The external Auger rates are highest for the largest possible overlap of the mesonic atom states, thus for small Δn , and $\Delta l = -1$. Hence, by this process the mesonic atom would tend to settle into circular orbits, in which $l = n-1$. Thus the intensity ratio of, say, K_α to the sum of all K-series x rays $K_\alpha / \sum K_J$ would be 0.8 or more when the cascade is along the circular level route. This means e.g., that the 2p level is much more heavily populated than are the higher p-states.

In solids the stripping process is checked by the rapid refilling of the empty internal electron levels from outside. Once the meson-nucleon system contains other electrons, the major de-excitation process shifts to the internal Auger effect, and the rates become relatively independent of the environment. The transition to this behavior occurs, from evidence on Stark-induced transitions to be given later, in the vicinity of lithium.

When n is small enough ($n \approx 5$ in helium), radiative

transitions begin to dominate the Auger transitions, and x-ray lines appear. In heavier elements the changeover occurs at higher n values, the radiation probability varying as Z^4 .

A. Collisional Stark Mixing. The ℓ -degeneracy of the hydrogenic levels in the mesonic atom is removed by any external field. In hydrogen and helium, in the absence of collisions, the degeneracy persists. Collisions can produce either a weak or a strong Stark-effect mixing process. In weak mixing, the levels are only slightly perturbed and retain their central-field identity; the main effect of the field is to induce dipole-type (sliding) transitions between neighboring sub-levels: $(n, \ell) \rightarrow (n, \ell+1)$. In strong mixing, the angular momentum quantum number is replaced by a new one measuring the angular momentum about the axis connecting the two nuclei (the molecular case) and accordingly all the different ℓ substates are mixed; in the case of strongly interacting mesons such as pions and kaons, this leads to immediate nuclear capture, through the admixture of s- and p-states.

B. Muonic Atoms. Because of the weak muon-nucleon interaction, muonic cascades can be used to determine the atomic mechanisms¹⁷⁻¹⁹ involved in the de-excitation of all types of mesonic atoms. In particular, the spectral intensity distribution within any x-ray line series provides information concerning the initial capture population and the cascade mechanisms producing the observed populations of various states. The cascade dynamics for pions and kaons can then be determined from the muon

cascade, taking into account reduced mass and nuclear absorption effects.

C. Pionics Atoms. Rapid nuclear absorption of the pion or kaon from atomic states leads to complex energy shifts of these levels²⁰⁻²² which can be related to the zero-energy pion- or kaon-nucleus complex scattering lengths. Thus, the interaction between negative mesons and nuclei at small kinetic energy can be studied by observing an mesonic x-ray spectrum.

A convenient representation of the complex pionic level shifts is given by the optical model theory of T.E.O. Ericson and M.Ericson.²³ Here the level shift is described by a pion-nucleus interaction potential related to pion-nucleon scattering and the pion-two nucleon (pair correlation) absorption potentials; the level width is determined by the imaginary part of the pion-two nucleon potential. A detailed exposition of this subject has recently been given by Burhop.²⁴

A study of the de-excitation cascades is particularly relevant to the question of nuclear absorption states. The gross behavior of the pion- or kaon de-excitation cascade is determined by the strong ℓ -dependence of nuclear absorption, which reflects the variation of meson-nucleus overlap with ℓ . Since pion d-state absorption rates are small compared to the radiative rates for low-Z nuclei, the L-series x-ray yield and spectral composition are essentially determined by the initial capture distribution and cascade mechanisms. The K-series yields depend strongly on 2p-state nuclear absorption

rates and decrease rapidly with increasing Z .

D. Kaonic Atoms. Because of the very strong absorption of kaons, resulting from the strong $\bar{K}N$ interaction, K-series x rays may not be observable, and the L-series x-ray yields will be very sensitive to the absorption rates in d-states. However, the spectral composition of all line series (L, M, N) ¹⁸ will reflect the initial capture distribution and cascade mechanisms.

In contrast, for low Z , the M-series x-ray yield is relatively independent of nuclear absorption rates--the f-state absorption being presumably negligible--but is sensitive to the initial capture distribution and the cascade mechanisms.

Of particular interest is the de-excitation cascade in He, in view of the measured long moderation time $(2.4 \pm 0.4) 10^{-10}$ sec, ²⁵ the kaon x-ray results of Burleson et.al. ¹, the results of the K^-_{α} elastic scattering experiments of Boyd et al. ², and Block et al. ³, and those of a recent π, μ x-ray experiment by Wetmore et al. ²⁶, which demonstrated an unexpectedly large population of non-circular orbits in low atomic levels. Thus new questions about the pion and kaon cascades and absorption in He have been raised.

E. Σ^- -Hyperonic Atoms. No previous experimental data have been available on Σ^- -atoms. The hyperon-nucleus interaction is strong; thus absorption from high excited states is to be ex-

pected, and in general, there should be a similarity to K-nucleus interactions. The fact that the spin of the sigma is $1/2$ and its magnetic moment non-vanishing leads to the possibility of seeing fine-structure effects of the sort observed in muon-capture spectra, and may some day lead to a direct experimental determination of the spin and magnetic moment.

VI. DISCUSSION OF RESULTS IN HELIUM

A. Muonic X Rays

The muon and pion work was undertaken initially to supplement and clarify the kaon He results, particularly the yields. The ZGS is not presently well suited to produce stopping pions or muons. From Table I it is clear that within their limited accuracy the energy measurements agree with earlier results. The muon x-ray yield data indicate, even with relatively large errors, that the K-series x-ray yields in He and Li are less than in Be and higher Z elements. Spurious decreases of this sort have been observed in the past, which disappeared when better data were obtained.²⁷ However, these data have survived all the tests we have been able to apply to them. They are also supported by independent observations--namely the anomalous intensity distributions in the muon and pion K-series, and the kaon L-series x rays for which a common explanation exists.

The De-excitation Cascade in Helium. Our data, like earlier experimental results,²⁶ indicate a low value of the

ratio, $K_{\alpha}/\Sigma K_{\beta}$ in He, which indicates a departure from predominantly circular orbit meson population.

To investigate further the meson-helium cascade process, a modified version of an earlier Monte Carlo computer program²⁸ was used. Given an initial population distribution, the program calculates the de-excitation cascade via hydrogenic energy levels of the $(\text{He-M})^{+}$ ion mentioned previously, allowing external (collisional) Auger and radiative transitions. The initial distribution is taken to be of the form $N(\ell) \sim (2\ell+1)\exp(-\alpha\ell)$,¹⁸ and the initial capture level is specified to be somewhere in the neighborhood of the electron K-shell, n is then about 12 for muons, 14 for pions, or 24 for kaons. The ion $(M\alpha)^{+}$ then de-excites according to the above scheme.

The program allows for meson-nucleus absorption in ns and np-states as described by the overlap integrals of these states with the nucleus. For muons, this absorption is eliminated and dipole transitions out of $n\text{sec}(n \geq 3)$ states are allowed. The original program allowed sliding transitions of only those circular orbits ($\ell=n-1$) with large n which are metastable because the external Auger transitions are not energetically allowed.

The experimental results (see Table I) on total muon K-series yield Y_K and intensity ratio $K_{\alpha}/\Sigma K_{\beta}$ provide boundary conditions for the cascade calculations. We found that no variation of the cascade starting level from $N_0 = 8$ to 15,

nor of the population distribution among different ℓ -value substates in the starting level, nor of the Auger transition rates by factors from 10^{-1} to 10 would give as large a K_{β} component (3p-state population) as observed, or as small a Y_K as observed.

To produce these results, mixing of the substate populations ("sliding transitions") must occur, which tends to equalize the populations of the low atomic states. Stark-effect (collisional) mixing provides such a mechanism.

Such transitions were first discussed in detail by Ruderman¹⁶ in connection with the "missing x-ray" problem in muonic atoms. He pointed out that the effect of sliding transitions would be to produce deviations from circular orbits, and showed that the electric field from two K-shell electrons was sufficient to produce the desired effect.

To investigate this, the cascade scheme was modified to allow Stark-induced dipole "polarization" transitions of the type $(n, \ell) \rightarrow (n, \ell \pm 1)$. The probability is assumed to be given, in the approximation of a constant average electric field during a collision, by

$$\text{const } x | \langle n, \ell \pm 1 | E \cdot \mathbf{r}_n | n, \ell \rangle |^2 = \langle F \rangle \left(R_{n, \ell}^{n, \ell \pm 1} \right)^2$$

where the rate parameter $\langle F \rangle$ specifies the time-averaged collisional strength, and $R_{n, \ell}^{n, \ell \pm 1}$ are the coulomb radial dipole matrix elements:

$$\left(R_{n, \ell}^{n, \ell - 1} \right)^2 = 9 \ell n^2 (n^2 - \ell^2) / 4(2\ell + 1),$$

and

$$\left(R_{n, \ell}^{n, \ell + 1} \right)^2 = 9(\ell + 1)n^2 \left(n^2 - (\ell + 1)^2 \right) / 4 \left(2(\ell + 1) + 1 \right).$$

Stark mixing of adjacent states was allowed to occur according to its probability relative to all transitions out

of the state (n, ℓ) .

This "sliding transition" approximation to the collisional mixing should be applicable for mixing rates small compared to the radiative and Auger rates, as the adjacent sub-levels are the most nearly degenerate states.

With the inclusion of Stark mixing, the cascade calculation could now reproduce the experimental results above, with a value of $\langle F \rangle$ about 10^8 sec^{-1} , representing rather weak collisions.

This mixing rate should not lead to a large population of higher s-states, or else the muon $K_\alpha / \Sigma K_J$ ratio would reach large values incompatible with experiment, because of $n s \rightarrow n' p \rightarrow n'' s \rightarrow 2p$ transitions. While the weak mixing provides adequate 3p, 2s populations, it does not seriously distort the cascade at higher levels.

The vacuum polarization effect for very low Z elements produces a splitting $E(2p \ 1/2) - E(2s \ 1/2)$ of 1.5 ev in He.¹⁶ Introducing collisional mixing enhances the allowed transition $2p \rightarrow 2s$, thus increasing the metastable 2s-state population in helium.

B. Pionic X Rays

For the pion cascade, nuclear absorption from the atomic s- and p-states has been added. The relative nuclear absorption rates for different n were determined by the ratio of the overlap integrals of the orbital wavefunctions with the nucleus;

$$\Gamma_{n,0}^c = 1/n^3 \Gamma_{1s}^c$$

and

$$\Gamma_{n,1}^C = (32/3) (1 - 1/n^2) 1/n^3 \Gamma_{2,1}^C; \Gamma_{2,1}^C \equiv \Gamma_{2p}^C.$$

We first tried the cascade without collisional mixing and with the 2p-state absorption rate $\Gamma_{2p}^C = 0$. For a range of starting levels $N_0 = 10, 15$ and initial capture distributions $\alpha = -0.25, 0.25$, the cascade predicts too large values for Y_K and $K_\alpha/\Sigma K_J$, while the K_β yield is too small. Allowing p-state absorption, the cascade will reproduce the experimental yield Y_K , but not the ratio $K_\alpha/\Sigma K_J$. (See Table VII).

As we found for the muons, there is no way to reproduce the experimental K-series yield and $K_\alpha/\Sigma K_J$ without introducing sliding transitions. With $\langle F \rangle \approx 10^8 \text{ sec}^{-1}$ (the same as for muons), the cascade produces results consistent with experiment for a 2p-state absorption rate $\Gamma_{2p}^C = (5 \pm 2) \cdot 10^{12} \text{ sec}^{-1}$, which is determined by the experimental K_α and K_β yields, and the assumed initial capture distribution. The K-series yields and $K_\alpha/\Sigma K_J$ values are sensitive to the p-capture rate, which explains the difference between the pion and muon spectral composition.

s/p Capture Ratio. For large n, the sliding transition rate required by the experimental results does not lead to pion absorption in high s-states, but allows most pions to reach low n levels where s-state capture is significant for $n < 5$. With the given Γ_{2p}^C , the ratio of s/p absorption with $\langle F \rangle \approx 10^8$, is 1.8. The same cascade without collisional mixing gives $s/p = 1.2$.

C. Kaon-Helium Results

Consider the null K^- -He results (Tables III, IV). Recent low energy K^- -He elastic scattering experiments^{2,3} have given kaon $1s$ -, $2p$ -state absorption rates $\Gamma_{1s}^c = 10^{19} \text{sec}^{-1}$ and $\Gamma_{2p}^c = 10^{15} \text{sec}^{-1}$ from the s - and p -wave scattering lengths determined from these data. A p -state absorption rate of this order would prevent the observation of K x rays for any p -state populations because the absorption so strongly dominates the radiation $\Gamma_{2p \rightarrow 1s}^{\text{RAD}} \leq 8.85 \cdot 10^{12} \text{sec}^{-1}$. (It was, in fact, this discrepancy with the high K_α and L_α yields reported by Burleson et al.¹) that led to this repetition of their experiment.

The experimental yield result $Y(L_\alpha)$ when combined with predicted (cascade) $3d$ -state populations, relates the $3d$ -state absorption rate and the radiative transition rate $\Gamma_{3d \rightarrow 2p}^{\text{RAD}} = 8.83 \cdot 10^{11} \text{sec}^{-1}$. In the absence of f -state absorption, the kaon-helium cascades predicts the following $3d$ -state populations: 17% for $\langle F \rangle \approx 10^8$, 5% for $\langle F \rangle \approx 10^9$, and 47% for $\langle F \rangle = 0.0$, i.e., no "sliding" transitions. Thus, in the absence of sliding transitions, the experimental one-standard deviation yield limit (10%) gives $\Gamma_{3d}^c \approx 3.2 \cdot 10^{12} \text{sec}^{-1}$. In the absence of collisional mixing, starting at $N_0 = 24$, with initial capture distributions which are not strongly skewed ($\alpha = -0.20$ to $\alpha = 0.20$) and a $2p$ -state capture rate $\Gamma_{2p}^c = 10^{15} \text{sec}^{-1}$, the cascade predicts that 90% or more of the kaons would be captured from np states with $n < 6$ because of the large populations in near circular orbits. With the same strength for sliding transitions as for pions ($\langle F \rangle \approx 10^8$),

the yield limit (10%) requires $\Gamma_{3d}^C = 5 \pm 2 \cdot 10^{11} \text{sec}^{-1}$. Such a cascade results in 20% absorption of kaons in s-states, about 7% in d-states, and the remainder in p-states. Increasing the mixing rate will decrease the 3d-state population and the inferred minimum Γ_{3d}^C absorption rate. Increasing the rate tenfold from that inferred for the pions i.e., to $\langle F \rangle \approx 10^9$, yields only a 5% 3d population, which is within the experimental yield limits on L_α even without 3d absorption; i.e., $\Gamma_{3d} = 0$. This leads to increased mixing into higher s-states, resulting in about 40% absorption of kaons from s-states.

These results indicate that s-state capture can only compete with p-state capture unless the collisional mixing rate is allowed to be larger than that considered.

Optical Model. It is possible to relate the 3d-state absorption rate Γ_{3d}^C and the 2p-state absorption rate Γ_{2p}^C . Because of the strong s-wave absorption in the $\bar{K}N$ interaction, given by $\text{Im } A(\bar{K}N)$,²⁹ and the absence of p-wave scattering at very low energy,³⁰ it is reasonable to consider a local s-wave, single-nucleon absorption model. We take

$$\Gamma_{n,l}^C = R \int \rho(r) |\psi_{n,l}|^2 d^3r$$

where $\rho(r)$ is the nuclear density described by the shell model nuclear charge distributions.³¹ Such a model assumes that the absorption does not severely perturb the coulomb wavefunctions. Then $\Gamma_{2p}^C/\Gamma_{1s}^C = 2.85 \times 10^{-4}$ and $\Gamma_{3d}^C/\Gamma_{2p}^C = 2.23 \times 10^{-4}$.

Using the 3d absorption rate $\Gamma_{3d}^C = 5 \pm 2 \times 10^{11} \text{sec}^{-1}$ inferred for $\langle F \rangle \approx 10^8$ the absorption relations give $\Gamma_{2p}^C \sim 2.7 \times 10^{15} \text{sec}^{-1}$ and $\Gamma_{1s} \sim 0.95 \times 10^{19} \text{sec}^{-1}$. In the absence of collisional mixing, $\langle F \rangle = 0.0$, using $\Gamma_{3d}^C \approx 3.2 \times 10^{12} \text{sec}^{-1}$, we would obtain $\Gamma_{2p}^C \approx 1.5 \times 10^{16} \text{sec}^{-1}$.

This result is to be compared with recent K^- -He scattering experiments. Boyd et al.² gave $\Gamma_{2p} = (1.1 \pm 0.4) \cdot 10^{15} \text{sec}^{-1}$ from the imaginary part of the p-wave phase shift. M. Block et al.³ have determined s-, p-, and d-wave phase shifts, whose imaginary parts predict a p-state absorption rate $\Gamma_p = (0.9 \pm 0.2) \cdot 10^{15} \text{sec}^{-1}$ and a d-state absorption rate $\Gamma_d = (1.7 \pm 0.5) \cdot 10^{10} \text{sec}^{-1}$. In order to agree with this d-state absorption rate, our L_α x-ray yield limit only requires a mixing rate ($F \approx 3 \cdot 10^8$), a predicted 25% s-state absorption of kaons. However, such a 3d-state absorption rate is lower than that suggested by an optical model fit to our 3d-state absorption rates derived from Li, Be, B, and C.³² But the kaon x-ray yield data in helium alone cannot exclude even higher mixing rates, e.g., $F \approx 10^9$, which predicts only a 5% 3d-state population and reduces the 3d-state absorption rate below our threshold for detection and while only increasing the s-state absorption to 35%.

D. Cascade Times

Pions. The cascade calculation ($\langle F \rangle = 0.0$) without sliding transitions yields a cascade time $\tau_c \approx 1.1 \cdot 10^{-11} \text{sec}$ for $N_0 \approx 14$; with sliding transitions and $\langle F \rangle = 10^8$ it gives

$\tau_C = 1.2 \times 10^{-11}$ sec. This is to be compared to the experimental moderation time $\tau_M = (3.19 \pm 0.23) \cdot 10^{-10}$ sec.³³

Kaons. The kaon cascade in He without sliding transitions ($\langle F \rangle = 0.0$) yields cascade times $\tau_C \approx 2.5 \times 10^{-11}$ sec for $N_0 = 20$ and $\tau_C \approx 4.6 \times 10^{-11}$ sec for $N_0 = 24$ for a statistical starting level population. Changing the initial distributions between $\alpha = -0.20$ and $\alpha = +0.20$ varies the cascade time about $\pm 10\%$. In the presence of "sliding" transitions $\langle F \rangle = 10^8$ we find $\tau_C \approx 3.0 \times 10^{-11}$ sec⁻¹ for $N_0 = 24$ and $\tau_C \approx 2.0 \times 10^{-11}$ sec⁻¹ for $N_0 = 20$ with a statistical population in both cases. These cascade times are to be compared with the experimental moderation time $\tau_M = (2.4 + 0.4) \times 10^{-10}$ sec.²⁵

The collisional mixing required by the present experimental results diminishes the possibility of trapping in the $(K - \alpha)^+$ cascade for near circular orbits for $n \gtrsim 16$ where dipole external Auger transitions are forbidden. Moving the cascade starting level above $N_0^+ = 24$ corresponds to kaon orbits in the $(K - \alpha - e)$ system, where an internal Auger transition may occur. For near-circular orbits dipole Auger transitions are energetically forbidden, but the mixing could depopulate these states rapidly.

However, J. Russel³⁴ has shown that in the $(K - \alpha - e)$ system, the l -degeneracy of the kaon atomic states of $n \approx 27$ is removed by the perturbation due to the non-central electron-kaon coulomb interaction. The energy splitting of the near circular orbits ($n \approx 27$) is ~ 0.5 eV. In such a case, these

states would not be mixed by a weak Stark effect, and trapping in the Wightman-Condo^{35,36} "doldrums" would be effective around $n = 27$, delaying the cascade for kaons in the near circular orbits, and offering a possible explanation for the long moderation times observed.

VII. MUON AND PION CAPTURE IN Li, Be, C

A. The Muon De-Excitation Cascade in Heavier Elements

The cascade program was adapted to heavier elements by replacing the external Auger transitions with internal K and L electron shell Auger dipole transitions.¹⁵ Both the K and L shell rates were made variable to allow for a possible K-shell Auger rate limitation by the L-shell external electronic Auger transition refilling rate, and to determine the influence of the direct L-shell Auger transitions.

The muon K- and L-series x-ray results in Li, Be, and C favor a cascade with the initial starting level ($N_0 = 14$) population slightly biased toward circular orbits, $\left(\alpha = 0.20 \begin{matrix} +0.10 \\ -0.20 \end{matrix} \right)$ as indicated in Table VII. The cascade predictions given correspond to calculated K- and L-shell Auger transition rates. Varying these rates by factor of 10^{-1} to 10 changes the ratio $X_\alpha / \sum X_J$ only a few percent. Direct L-shell transitions are required by energy conservation in order to allow Auger transitions in higher ($n \geq 10$) levels. The predicted Y_K result from populating the assumed metastable 2s-state.

B. Like Pion De-Excitation Cascades in the Solid Elements

As with the muons, both internal K- and L-shell Auger transitions were considered. The program included s- and p-state absorption effects. Variation of the Auger rates by factors of 10^{-1} to 10 had little effect on the K- and L-series x-ray yields; it influenced mainly the relative yields of higher (β, γ) components of the x-ray line series.

The strong dependence of L x-ray yields on the initial starting level population distribution indicated that a distribution slightly biased toward circular orbits ($\alpha = 0.20^{+0.10}_{-0.20}$) is required by the experimental Y_L in Be and C, (Table VII). The experimental ratio $K_\alpha / \Sigma K_J$ in Li also favors the $\alpha = 0.20$ distribution.

2p-State Linewidths Using the cascades to predict 3d- and 2p-state populations, the experimental K-series x-ray yields establish 2p-state absorption rates in He, Li, Be, and C. These rates, and also some recent results of Koch et al.,³⁷ are given in Table II. These experimental pion 2p-state absorption rates can be compared to the absolute rates predicted by the optical model of T.E.O. Ericson and M. Ericson.²³ In that model, the absorption width (rate) of a level (n, l) is given by

$$\Gamma_{n,l}^C = A_1 \int \rho^2(r) |\psi_{n,l}|^2 d^3r + A_2 \int \rho^2(r) |\Delta\psi_{n,l}|^2 d^3r$$

where the first term corresponds to the s-wave part and the second to the p-wave part of the pion-two nucleon optical potential. The constants A_1, A_2 , taken from D. Jenkins, et al.³⁸

were determined from a fit to their data for the width of the 2p, 3d, 4f states in intermediate and high-Z pionic atoms. These values agree well with those calculated by M. Ericson from pion production by two nucleons. For calculational purposes, the nuclear density has been taken to be described by nuclear shell-theory charge distributions.³¹ A comparison of the experimental Γ_{2p}^C and the absolute rates determined by the optical model are given in Table II and shown in Fig. 11.

1s-State Level Shifts and Line Widths. While no pion K_α x-ray energy shift has been detected in He, energy shifts have been observed in Li and Be (Table II). Because of the large instrumental line widths and muon contamination effects, natural line broadening was detected only in Be, while limits are given in Li and He. The best K_α line width limit in helium comes from Wetmore et al.²⁶, $\Gamma_{1s}^C < 1.3 \times 10^{17} \text{ sec}^{-1}$.

An independent estimate of the 1s-state line width in helium can be obtained from the 2p-state absorption rate derived from the cascade calculations, and the ratio of 2p- to 1s-absorption rates given by overlap integrals. The result is $\Gamma_{2p}^C / \Gamma_{1s}^C \approx 1.6 \times 10^{-4}$. The experimental K-series x-ray yield data and cascade calculations indicate that $\Gamma_{2p}^C = (5.0 \pm 2.0) \times 10^{12} \text{ sec}^{-1}$ which gives $\Gamma_{1s}^C = 3.1 \pm 1.2 \times 10^{16} \text{ sec}^{-1}$.

Table II provides a comparison of the experimental pion K x-ray results with the theoretical energy shift and line-width predictions of the optical model²³ and the line-width predictions of the two-nucleon absorption model.²⁰ The

experimental 1s level widths are consistent with the predictions of the two-nucleon absorption model.

VIII. KAON Li, Be AND C RESULT

Examples of spectra are shown in Figs. 12, 13, and 14. The results of fitting line shapes to all the structure in these spectra are given in Table V. Within this set the M'_α line in C, the L'_α line in Be, and L'_α , L'_β lines in Li have been identified. The measured energies of these lines agree with the corresponding Klein-Gordon energies. Since the vacuum polarization and nuclear finite size corrections are very small in the 2p, 3d, 4f, etc. states, the good agreement of the experimental and theoretical energies indicates the absence of large nuclear absorption energy shifts of the levels involved.

A. Additional Lines in the X-Ray Spectra

The additional statistically significant resolved structure in these spectra consists of an M'_α (18.45 keV) line in C, and L'_β (18.00 keV) and L'_α (12.90 keV) in Li, and a possible L'_α (21.00 keV) in Be (where the terminology is arbitrary).

The additional line in C is also indicated in the spectrum of Wiegand and Mack³⁹. From a strictly statistical standpoint, these lines are present to confidence levels of 99% or better. We have considered the following possibilities as sources of these lines:

1. Background Effects. These lines are absent from the corresponding no-target and out-of-time (random) background spectra. Because of the purity (>99%) of the stopping K^- signal,⁷ this indicates that the lines are associated with kaons stopping in the targets.

2. Additional Kaon X-Ray Lines Due to Nuclear Effects. The L-series could be split if the (3p→2s) and (4p→2s) transitions differ in energy from the L_α (3d→2p) and L_β (4d→2p) lines, as a result of a nuclear interaction shift of the 2s-state. (See Fig. 15). If this is true, the measured energy and width of the 2s-state can be scaled with overlap integrals to find the corresponding parameters for the 1s-state. The resulting 1s-state is well defined (width and energy shift small compared to the binding energy). We then expect to see the K_β and K_γ transitions to the 1s-state from the 3p- and 4p-states, with rates predictably greater than those to the 2s-state. But such lines are not observed.³⁹ Moreover, the p- and d-state nuclear absorption rates inferred from the cascade calculations described below are large and do not allow such an interpretation.

The possibility that the additional line in the C spectrum could be a shifted M_α transition (4d→3p) is similarly ruled out.

3. Miscellaneous. We have not been able to identify these lines as nuclear gamma rays, fluorescence x rays, or as escape peaks from higher energy x-ray lines.

4. Secondary Pion X-Ray Lines. Absorbed kaons produce

negative pions which when stopped emit pionic x rays. Pion capture in counters, moderators, etc. can be excluded because all the observed lines are target dependent. Capture in the targets should yield characteristic pion spectra, but only in carbon can an observed line be identified with a prominent (L_{α}) pion target capture line. However, an equally thick Be target shows no Be pion lines, and one would have to postulate significant differences in the pion yield or spectra in the two elements to explain this. The lines observed in Li cannot be fitted to pion capture x-rays. Wiegand and Mack³⁹ also saw this line in C, since they used thinner targets, this tends to argue against the pionic interpretation of its origin.

5. Σ^{-} Atoms. In the absence of experimental data on Σ^{-} yields following K^{-} capture in Li, Be, and C, we interpolate between the measured yields of Σ^{-} hyperons from kaon capture in helium and heavy-liquid bubble chambers⁴⁰ to find that about 15% of stopped kaons should produce Σ^{-} hyperons. Assuming the same Σ^{-} momentum spectrum as that observed in helium,⁴⁰ we find that about 50% of the Σ^{-} 's produced would stop in our Li target. The uncorrected Dirac energies of the M_{α} and M_{β} transitions of Σ^{-} x rays in Li are 11.8 and 17.2 keV. If we identify the additional lines in the Li spectrum with these, we require a downward (attractive) energy shift of the 3d state of 0.95 ± 0.30 keV, which is not unreasonable. The respective M_{α} and M_{β} yields are 0.4 ± 0.2 and 0.7 ± 0.4 , which again are reasonable.

The Be spectrum is consistent with the presence of the $\Sigma^- M_\alpha$ (21.7 keV, unshifted) line also, as well as unresolved low energy kaon or Σ^- N-series lines. The yield would be $Y_{M_\alpha} = 0.8 \pm 0.4$. In C, the situation is less clear, however. The 18.45 keV line would have to be identified (implausibly) as an unshifted Σ^- ($10 \rightarrow 6$) transition (18.4 keV), or as a shifted Σ^- ($5 \rightarrow 4$) transition (23.3 keV) or Σ^- ($7 \rightarrow 5$) transition (20.3 keV). The yield, estimated as above, would be (0.8 ± 0.4) .

In the case of Li the interpretation as sigma-capture x rays appears the most plausible. The evidence in Be is more equivocal, but favors the interpretation as sigma M_α . In C the interpretation as a pion capture line seems most likely. If sigma lines appear, some pion lines could also appear, so these are not necessarily conflicting. Clearly more data with improved resolution are needed.

B. Cascade Calculations in Li, Be and C

The modified cascade program, adapted to higher Z values, as previously described for the pion cascades, was used to derive d-state absorption rates.

Cascade in Be. The L_α yield is essentially independent of the starting level N_0 , p-state absorption rates, and Auger transition rates. A statistical capture distribution ($\alpha=0.0$) predicts a yield of $L_\alpha = 0.19$, marginally consistent with the experimental yield 0.23 ± 0.03 even assuming no d-state absorption.

Taking $\alpha = 0.20$ for the initial capture population, and neglecting 3d-state absorption, the cascade predicts an L_α yield of 0.37. From the experimental yield $\Gamma_{3d \rightarrow 2p}^{\text{RAD}}$ we obtain a 3d-state absorption rate (Table V).

The observed upper limit to the natural line width of the L_α x-ray ($\Gamma_n < 0.22$ keV) establishes an upper limit on the 2p-state absorption (Table V).

Cascades in C. The 4f-state population determines the M_α x-ray yield. For $\alpha = 0.20$, the cascade-predicted 4f-state population (0.37) is consistent with the experimental yield (0.34 ± 0.07) and establishes an upper limit of the 4f-state absorption rate: $\Gamma_{4f}^{\text{C}} < 2.5 \cdot 10^{12} \text{ sec}^{-1}$. A statistical capture distribution ($\alpha = 0.0$) predicts a smaller M_α yield (0.22) than that observed even in the absence of the 4f-state absorption.

From the results of Wiegand and Mack³⁹, the L_α yield is less than 0.04 in C. Taking $\alpha = 0.20$ for the initial capture population and neglecting 4f-state absorption, the cascade gives $L_\alpha = 0.38$. From the yield limit 0.04, and $\Gamma_{3d \rightarrow 2p}^{\text{RAD}}$, we obtain a lower limit on the 3d-state absorption rate (Table V). Absorption from the d-states will not seriously affect the 3d-state population given by the cascade as $\ell \rightarrow \ell - 1$ transitions dominate. An upper limit on the 3d-state absorption can be obtained from the natural line width of the M_α x-ray ($\Gamma_n < 0.40$ keV). (Table V).

Taking $\alpha = 0.20$ for the initial capture distribution as suggested by the pion data, the cascade without d-state absorption predicts a yield of 0.37. From the observed value 0.09 ± 0.03 , and $\Gamma_{3p \rightarrow 2p}^{\text{RAD}}$, we obtain a 3d-state absorption rate (Table V). This d-state absorption rate will reduce the predicted $L_\alpha / \Sigma L_J$ from 0.70 to a value ≈ 0.60 for $\alpha = 0.20$, because of the differing absorption in the 3d and 4d-states given by the overlap integrals; this value is in agreement with the observed $L_\alpha / \Sigma L_J = (0.55 \pm 0.10)$.

Although limited in accuracy, the L_α , L_β line-width measurements yield a natural line-width upper limit

$$\Gamma_n < 0.30 \text{ keV and a } 2p\text{-state absorption rate (Table V),}$$

$$\Gamma_{2p}^c < 4.7 \times 10^{17} \text{ sec}^{-1}.$$

Comparison With Other Data

A comparison of the present yield results with those of Wiegand and Mack³⁹ in Fig. 16 indicates that the most obvious difference in the results of the two experiments lies in the trend of the L_α yield vs Z. Our results imply a maximal L_α yield in Be with the yield decreasing in Li toward zero in He. The results of Wiegand and Mack indicate, minimally, no decrease in L_α yield in going from Be to Li. However, the total L yields for the two experiments are consistent. The present kaon-helium L x-ray result, and the observed $K_\alpha / \Sigma K_J$ and Y_K for pions and muons, would suggest a decrease in L_α , Y_L for kaons in Li compared to Be.

Figure 17 illustrates the experimental kaon 3d-state absorption rates vs Z compared to those predicted by the s-wave overlap integrals normalized to the lower limit on the carbon 3d-state absorption rate, and to the absolute absorption rates calculated by J. Rook^{4 1} following the model of E.H.S. Burhop^{4 2} based on $\bar{K}N$ absorption cross sections. The kaon 3d-states absorption rates, as here determined, seem reasonably well described by the simple s-wave $\bar{K}N$ optical absorption model.

IX. SUMMARY

In conclusion, the present experimental results for muons indicate that muonic atoms in the light elements can be understood in terms of the normal electromagnetic de-excitation cascade dominated by internal Auger transitions, with an initial capture distribution slightly biased toward circular orbits ($\alpha = 0.20 \pm 0.10$), and the metastability of the muonic 2s-state.

The biasing of the initial capture distribution, required for the cascade starting at or below the electron K-shell radius, may be a reflection of processes following initial capture in higher n levels. Energy conservation in Auger transitions of the muons from near circular orbits in these higher n levels requires a large Δn and Δl as described. As the transition rate decreases rapidly with increasing Δl , muons in such states will de-excite with a minimum Δl and thus tend to enrich the population of the

near circular orbits in the lower part of the cascade (below the electron K shell).

For helium, the muon results can be explained only by invoking weak collisional Stark effects. In particular, for an initial statistical capture distribution, the experimental muon K-series x-ray results can be reproduced by a cascade involving external Auger and radiative transitions along with weak (adjacent state $n, \ell \rightarrow n, \ell + 1$) Stark mixing.

The preference for an initial statistical capture distribution for the cascade calculations in helium may reflect the effect of the Stark mixing on the populations of atomic states given by initial capture at higher n levels.

Again, for pions the same conclusions apply, with the addition of nuclear absorption from atomic s and p-states. Cascade calculations, in conjunction with the experimental pion K-series x-ray yields, give pion 2p-state absorption rates in agreement with the optical model of T.E.O. Ericson and M. E. Ericson.²³ The same model predicts 1s-state energy shifts and absorption rates in good agreement with the experimental results.

For kaons, the identified kaonic x-ray results in the light elements can likewise be understood in terms of the normal de-excitation cascade with the same initial capture distribution biased toward circular orbits $\left(\alpha = 0.20_{-0.20}^{+0.10} \right)$ and 3d-state absorption rates describable by a simple optical model.

In helium, the kaon null results can be understood by invoking the same amount of collisional mixing as required by muons and pions, and a 3d-state absorption consistent with the 1s, 2p absorption rates and ratio Γ_{2p}/Γ_{1s} given by recent kaon- α elastic scattering experiments. They provide significant, but not definitive, information concerning the amount of s-, p- and d-state capture, and the experimental moderation time; they do not establish an upper limit on the collisional mixing rate for the $(K\alpha)^+$ system.

The additional line structure in the kaon Li and Be spectra is consistent with and apparently explicable only as M-series Σ^- x-ray lines. The line in the kaonic c-spectrum seems to be best described as the pionic L_{α} x-ray line.

It is clear that in neither pionic nor kaonic helium atoms does nuclear capture occur exclusively from a single state; it occurs from states with two or three different ℓ -values.

X. ACKNOWLEDGMENTS

For the use of the helium target, and for interesting suggestions, we thank Prof. R. A. Schluter. For his design and setup of the electronics and general engineering assistance, we are grateful to William Rickhoff. For his untiring assistance in the construction, testing, installation and operation of the equipment, we are greatly indebted to Don Jankowski. For valuable discussions of the experiment we are grateful to Dr. J. Uretsky, Prof. M. M. Block, and Prof. Valentine L. Telegdi. The operation of the equipment was greatly facilitated by the help of the ZGS floor crew, and especially by Mr. William Siljander.

REFERENCES

- ¹G. Burleson, D. Cohen, R. Lamb, D. Michael, R. A. Schluter, and T. O. White Jr., Phys. Rev. Letters, 15, 70 (1965).
- ²J. Boyd, R. Burnstein, J. McComas, V. Viers, and G. Rosenblatt, Phys. Rev. Letters 19, 1406 (1967).
- ³P. O. Mazur, M. M. Block, J. Keren, and S. L. Meyer, Phys. Rev. (in press).
- ⁴S. Berezin, G. Burleson, D. Eartly, A. Roberts, T. O. White Jr., Phys. Letters 27, 308 (1969).
- ⁵A. Roberts, Proc. 3rd Annu. Rochester Conf. on High Energy Physics (Interscience, 1952, pg. 93).
- ⁶T. DAY, G. Snow, T. Sucher, Phys. Rev. Letters 3, 61 (1959); Phys. Rev. 118, 864 (1960).
- ⁷A. Roberts, D. Eartly, Nucl. Instr. and Methods, 73, 336 (1969).
- ⁸Reuter-Stokes, Cleveland, Ohio.
- ⁹A.N.L. Electronics Div. A-162.
- ¹⁰A.N.L. Electronics Div. LPA-19.
- ¹¹A.N.L. Electronics Div. LPS-100.
- ¹²A.N.L. Electronics Div. G-187.
- ¹³R. Lamb, R. A. Schluter, D. Michael, A. Tamosaitis, H. Ludwig, Bull. Am. Phys. Soc. 9, 640 (1964).
- ¹⁴As pointed out by R. A. Schluter, A.N.L. and Northwestern University.
- ¹⁵G. R. Burbidge, A. H. deBorde, Phys. Rev. 89, 189 (1952).
- ¹⁶M. Ruderman, Phys. Rev. 118, 1632 (1960).
- ¹⁷M. Leon, H. Bethe, Phys. Rev. 127, 636 (1962).
- ¹⁸Y. Eisenberg, D. Kessler, Nuovo cimento 20, 1195 (1960); Phys. Rev. 123, 1472 (1961) and Phys. Rev. 130, 2352 (1963).

- ¹⁹J. Bernstein, T. Y. Wu, Phys. Rev. Letters 2, 404 (1959),
and N. Kroll, E. Gerjuoy, Phys. Rev. Letters 3, 142 (1959).
- ²⁰K. Brueckner, Phys. Rev. 98, 769 (1955); S. Deser, M.
Goldberger, K. Baumann, W. Thirring, Phys. Rev. 96, 774 (1954);
and N. Byers, Phys. Rev. 107, 843 (1957).
- ²¹T. Trueman, Nucl. Phys. 26, 57 (1961).
- ²²F. Von Hippel, J. Douglas, Phys. Rev. 146, 1042 (1966) and
J. Uretsky, Phys. Rev. 147, 906 (1966).
- ²³M. Ericson, T.E.O. Ericson, Ann. Phys. 36, 323 (1966);
M. Ericson, C. R. Acad. Sci. 258, 1471 (1963).
- ²⁴E.H.S. Burhop, High Energy Physics, Vol. III, p. 110,
(Academic Press, New York (1969)).
- ²⁵M. M. Block, J. Kopelman, C. Sun. Phys. Rev. 140, 143 (1965).
- ²⁶R. Wetmore, D. Buckle, J. Kane, R. Siegel, Phys. Rev. Letters,
9, 1003 (1967).
- ²⁷J. Lathrop, R. Lundy, V. L. Telegdi, R. Winston, Phys. Rev.
Letters, 7, 147; and M. B. Stearns, Bull. Am. Phys. Soc. 9,
81, (to be published).
- ²⁸D. N. Michael, Phys. Rev. 158, 1343 (1967).
- ²⁹D. Basu, S. Biswas, K. Dutta, Phys. Rev. 176, 1840 (1968).
- ³⁰Jae Kwan Kim, Phys. Rev. Letters, 19, 1074 (1967).
- ³¹"Landolt-Bornstein, Nuclear Radii, Vol. 2.
- ³²S. Berezin, G. Bureson, D. Eartly, A. Roberts, T.O.White
Jr., Nucl. Phys. (in press).
- ³³M. M. Block, T. Kikuchi, D. Koetke, J. Kopelman, C. Sun.
R. Walker, G. Culligan, V. L. Telegdi, R. Winston, Phys. Rev.
Letters, 11, 303 (1963); J. Fetkovich, E. Pewitt, Phys. Rev.
Letters, 11, 290 (1963).
- ³⁴J. E. Russell, Phys. Rev. (in press).
- ³⁵A. S. Wightman, Thesis, Princeton Univ., 1949; Phys. Rev.
77, 521 (1950).
- ³⁶G. Condo, Phys. Letters, 9, 65 (1964).

- ³⁷H. Koch, G. Poelz, H. Schmitt, L. Tauscher, G. Backenstoss, s. Charalambus, H. Daniel, Phys. Letters, 28, 279 (1968).
- ³⁸D. Jenkins, R. Kunselman, Phys. Rev. Letters, 17, 1148 (1966); D. Jenkins, K. Crowe, Phys. Rev. Letters, 16, 637 (1966).
- ³⁹C. Wiegand, D. Mack, Phys. Rev. Letters, 18, 685 (1967).
- ⁴⁰B. Riley, Bull. Am. Phys. Soc. 14, private communication.
- ⁴¹J. R. Rook, Nucl. Phys. 9, 441 (1968).
- ⁴²E.H.S. Burhop, Nucl. Phys. 1, 438 (1967).

TABLE I. MUON X-RAY YIELDS

Element	Line	Line Energy (keV) (observed)	Total Series Yield (Y_K, Y_L)	Relative Intensity ^a $R_\alpha = K_\alpha / \sum K_J$
He	K_α	8.25 ± 0.15	0.79 ± 0.13	0.58 ± 0.05
	$K_{\beta, \gamma}$	9.90 ± 0.15^b		
Li	K_α	18.75 ± 0.15	0.75 ± 0.15	0.72 ± 0.05
	$K_{\beta, \gamma}$	22.20 ± 0.03		
Be	K_α	33.25 ± 0.15	1.09 ± 0.13	0.83 ± 0.07
	K_β	39.55 ± 0.15		
	L_α	6.20 ± 0.32	0.38 ± 0.09^c	- -
C	L_α	14.06 ± 0.32	0.50 ± 0.10	0.83 ± 0.07
	L_β	19.08 ± 0.32		

a) Corrected for relative detection efficiency.

b) Indicates a small γ component.

c) $Y_{L_\alpha} = 0.33$. Because of the μK_β Xenon K_α escape peak, Y_{L_β} cannot be determined, but is assumed to be $0.15 Y_{L_\alpha}$.

TABLE II. PION X-RAY YIELDS AND 1s, 2p-STATE ABSORPTION RATES

Element	Line	Line Energy (keV) (observed)	Total Series Yield (Y_K, Y_L)	Relative Intensity ^a $R_\alpha = K_\alpha / \Sigma K_J$	Energy Shift ΔE_{1s}	Width of K_α Line (keV)
He	K_α	10.80 ± 0.15	0.18 ± 0.05	0.40 ± 0.05	---	
	K_β	12.85 ± 0.15^c				
Li	K_α	24.11 ± 0.22	0.21 ± 0.05	0.70 ± 0.06	0.52 ± 0.22	$\leq 0.19^d$
	K_α	42.30 ± 0.15	0.21 ± 0.05		1.64 ± 0.15	0.70 ± 0.40^d
Be	L_α	8.10 ± 0.15				
	L_β	10.80 ± 0.25	0.35 ± 0.07	0.90 ± 0.06^b		
C	L_α	18.40 ± 0.32	0.36 ± 0.10	0.84 ± 0.07		
Element		1s-State Absorption Rate Γ_{1s} (sec ⁻¹)	2p-State Absorption Rate Γ_{2p} (sec ⁻¹)			
He		$(1.9 \pm 1.2) \cdot 10^{17}$	$(3.0 \pm 2.0) \cdot 10^{12} e$			
Li		$\leq 2.9 \cdot 10^{17}$	$(2.5 \pm 1.0) \cdot 10^{13}$			
Be		$(1.06 \pm 0.58) \cdot 10^{18}$	$(8.0 \pm 2.0) \cdot 10^{13}$			
C		---	$(1.9 \pm 0.3) \cdot 10^{15}$			

- a) Corrected for relative detection efficiencies.
- b) Determined from the limit on the K_β escape peak.
- c) Best fit energy assuming instrumental linewidth and a γ component of 10% intensity.
- d) Lorentzian Line Width.
- e) Determined from yields and cascade calculations.

TABLE III. YIELDS OF K-SERIES X-RAYS FROM KAON CAPTURE IN HELIUM.

Klein-Gordon Energy-(keV)	Yield for Unshifted Line of Instrumental	Yield for Shifted Line		Yield for Shifted Line Line $\Delta E = -2.0$ keV $\Gamma = 2.0$ keV	Yield for K_{α} $\Delta E = +6.0$ keV $\Gamma = 6.7$ keV
		$\Delta E = +2.0$ keV $\Gamma = 2.0$ keV			
A. Target Full minus Target Empty Yields.					
K_{α} 34.9	0.06±0.05	0.06±0.05	0.13±0.10	0.08±0.07	
K_{β} 41.3	0.02±0.07	0.02±0.07	0.03±0.07		
eK_{β} 11.7 (escape)	0.15±0.12	0.10±0.08	0.28±0.20		
B. Target Full: Signal minus Out-of-Time Background Yields.^b					
K_{α}	0.09±0.05	0.07±0.06	0.17±0.08		
K_{β}	0.10±0.06	0.10±0.07	0.11±0.06		
eK_{β}	0.07±0.05	0.06±0.05	0.20±0.12		

a) As predicted from scattering data of Reference 3.

b) This difference spectrum yield is dependent on spectrum matching regions.

TABLE IV. YIELDS OF L-SERIES X-RAYS FROM KAON CAPTURE IN HELIUM.

Klein-Gordon Energy (keV)	Yield for Unshifted Line	Yield for Line	
		Shifted $\Delta E = +0.5$ keV	Shifted $\Delta E = -0.5$ keV
Long minus short coincidence gate data: target full minus target empty			
L_{α} 6.5	0.03 ± 0.07	0.03 ± 0.07	0.07 ± 0.10
L_{β} 8.7	0.03 ± 0.04	0.03 ± 0.04	0.03 ± 0.05

TABLE V. X-RAY LINES FROM KAON CAPTURE IN Li, Be, AND C AND 3d-STATE ABSORPTION RATES.

Element	Line	Energy (keV)	Total Series Yield (Y_L, Y_M)	Yield α -Line	Relative Intensity $R_\alpha = L_\alpha / \sum L_j$	3d-State Absorption Rate Γ_{3d} (sec^{-1})
Li	L_α	15.00 ± 0.30	0.16 ± 0.05 ^a		0.55 ± 0.1	$(1.45^{+0.90}_{-0.48}) \cdot 10^{13}$
	L_β	20.80 ± 0.30				
	" L_α " ^b	12.90 ± 0.30	0.08 ± 0.03			
	" L_β "	18.00 ± 0.30				
Be	L_α	27.50 ± 0.30	$0.28^{+0.14}_{-0.06}$	$\alpha = 0.23 \pm 0.03$	$0.82^{+0.10}_{-0.20}$	$(0.93^{+0.36}_{-0.29}) \cdot 10^{13}$
	" L_α " ^b	21.00 ± 0.30	0.10 ± 0.03			
C	M_α	22.30 ± 0.30	0.44 ± 0.10	$\alpha = 0.34 \pm 0.07$	0.77 ± 0.10	$< 6.0 \cdot 10^{14}$ $> 7.3 \cdot 10^{17}$
	" M_α " ^b	18.45 ± 0.30	0.10 ± 0.03			
He						$(6.0 \pm 2.0) \cdot 10^{11}$

a) This yield corresponds to the α, β lines only.

b) Quotes indicate phenomenological terminology; for identification of these lines see Sec. VIIIA.

TABLE VI. HELIUM CASCADE RESULTS.

NAL-37

1111

<u>Muons</u>		<u>Calculated</u>		<u>Experimental</u>
$N_O=13, \alpha=0.0^a$	F=0	F=10 ⁸		
Yield Y_K	0.97	0.80		0.79±.13
Ratio $K_\alpha/\Sigma K_J$	0.73	0.55		0.58±.05
<u>Pions</u>				
$N_O=13, \alpha=0.0$				
Yield Y_K	0.34	0.21		0.18±.05
Ratio $K_\alpha/\Sigma K_J$	0.63	0.40		0.40±.05
Ratio, p/s-state capture	1.8	1.2		
<u>Kaons</u>				
$N_O=20, \alpha=0.0$	F=0	F=10 ⁸	F=10 ⁹	
3d popul.	47%	16%	5%	
$\Gamma_{3d}^c, \text{sec}^{-1}$	>3.2.10 ¹²	>(5.0±2.0).10 ¹¹	→0	
$\Gamma_{2p}^c, \text{sec}^{-1}$	>1.4.10 ¹⁶	>(2.3±0.8).10 ¹⁵	--	
<u>Nuclear Absorption for Experimental Yields</u>				
d-state	30%	7%	→0	
p-state	69%	73%	65	
s-state	1%	20%	35	
From K^- -He Scattering Data: Boyd et.al. Ref. 2 Mazur et.al Ref.3				
Γ_{2p}^c		(1.1±.4)x10 ¹⁵ sec.	(1.43±.29)x10 ¹⁵ sec ⁻¹	
Γ_{3d}^c			3.8±1.0 .10 ¹⁰ sec ⁻¹ 2.9±0.9	
		Calculated Cascade Time	Moderation Time	
Pions		1.2.10 ⁻¹¹ sec.	(3.2±0.2) .10 ⁻¹⁰	
Kaons		3.0.10 ⁻¹¹	(2.4±0.4) .10 ⁻¹⁰ sec	

- a) Skewing parameter of Eisenberg and Kessler. Ref. 18.
- b) Reference 33.
- c) Reference 25.

TABLE VII. EXPERIMENTAL vs. CASCADE CALCULATION YIELDS.

	EXPERIMENTAL RESULTS		CASCADE PREDICTIONS ^a		EXPERIMENTAL RESULTS		CASCADE PREDICTIONS	
	Y_K	$K_\alpha/\Sigma K_J$	Y_K	$K_\alpha/\Sigma K_J$	Y_L	$L_\alpha/\Sigma L_J$	Y_L	$L_\alpha/\Sigma L_J$
<u>MUONS</u>								
He	0.79 ± 0.13	0.58 ± 0.05	0.97 0.80	0.73 ^b 0.55 ^c				
Li	0.75 ± 0.15	0.72 ± 0.05	0.81 0.85 ^d	0.62 0.71 ^d				
Be	1.09 ± 0.13	0.83 ± 0.07	0.88 0.89 ^d	0.59 0.62 ^d	0.38 ± 0.09	--	0.27 0.28 ^d	0.87 0.89 ^d
C					0.50 ± 0.10	0.83 ± 0.07	0.42 0.51 ^d	0.78 0.85 ^d
<u>PIONS</u>								
He	0.18 ± 0.05	0.40 ± 0.05	0.34 0.21	0.63 ^e 0.40 ^f				
Li	0.21 ± 0.05	0.70 ± 0.06	0.25 ^d	0.50 0.60				
Be	0.21 ± 0.05	0.90 ± 0.06	0.20 ^d	0.50 0.62 ^d	0.35 ± 0.07	0.80 ± 0.06	0.21 0.33 ^d	0.82 0.88 ^d
C					0.36 ± 0.10	0.84 ± 0.06	0.33 0.50 ^d	0.75 0.82 ^d

- a) Statistical capture distribution is assumed unless noted.
- b) Helium cascade without collisional mixing.
- c) Helium cascade with collisional mixing; $F = 10^8$
- d) Biased circular orbit scheme; $\alpha = 0.20$, for initial capture.
- e) No collisional mixing but $\tau_{2p}^C = 3.0 \cdot 10^{-12}$ sec.
- f) Collisional mixing and $\tau_{2p}^C = 3.0 \cdot 10^{-12}$ sec.

Figure Captions

Fig. 1. a) Counter arrangement for stopping kaons. C_1 and C_2 are Cerenkov counters in a time-of-flight circuit to select kaons; S_1 and S_2 are scintillation counters, S_3 is a pulse-height discriminating scintillator, to emphasize slow kaons emerging from the moderator, and ACDS is a downstream anticoincidence counter following the target T. The eight proportional counters PC_j detect x-rays; they are protected from charged fragments by the anti-coincidence counters AC_j . b) Arrangement for stopping muons and pions; the time-of-flight Cerenkov counters are replaced by the gas threshold Cerenkov counter C_G , which discriminates between muons and pions.

Fig. 2. Simplified slow electronics for the proportional counter x-ray spectrometer. Each of the four channels has its own quadrant of the pulse height analyzers, and its own pulse shaping and pulse rejection system.

Fig. 3. Delay variation in the high-pressure xenon proportional counters as a function of x-ray energy. The increased delay at low energies is due to absorption in the outer low-field region of the counters.

Fig. 4. Muon spectra in helium. a) Muon-helium capture spectrum minus same data for empty target. b) Muon-helium capture spectrum minus random background (out-of-time spectrum).

- Fig. 5. Pion-helium capture spectrum minus random (out-of-time) background.
- Fig. 6. Kaon capture in helium. a) Signal plus background.
b) Background only.
- Fig. 7. Kaon-helium capture spectrum minus same data for empty target.
- Fig. 8. Kaon-helium data with 4- μ sec gate width. a) Random (out-of-time) spectrum minus dummy target random spectrum (the difference represents non-beam-associated x-rays from helium). b) Helium data minus dummy target data (the difference represents beam-associated x-rays from helium).
- Fig. 9. Kaon-helium data with 4- μ sec gate. Kaon-helium capture spectrum minus random (out-of-time) background.
- Fig. 10. Difference between kaon-helium capture data with 4- μ sec gate and 2.5- μ sec gate; only low energy x-rays should appear.
- Fig. 11. Comparison of experimental 2p pion absorption rates (partly derived from Monte Carlo calculations) and theoretical predictions.
- Fig. 12. X-ray spectra from kaon capture in lithium. a) Target in minus target out. b) In-time data minus random (out-of-time) data.
- Fig. 13. X-ray spectra from kaon capture in beryllium. a) In-time data minus random (out-of-time) data.
b) Target in minus target out.

Fig. 14. Same as Fig. 13, for capture in carbon.

Fig. 15. Elimination of level shift as source of additional spectral lines.

Fig. 16. L-series X-ray yields from kaon capture in light elements: total L-series yield, and L_{α} yields.

Fig. 17. Comparison of experimental and theoretical 3d kaon absorption rates in light elements.

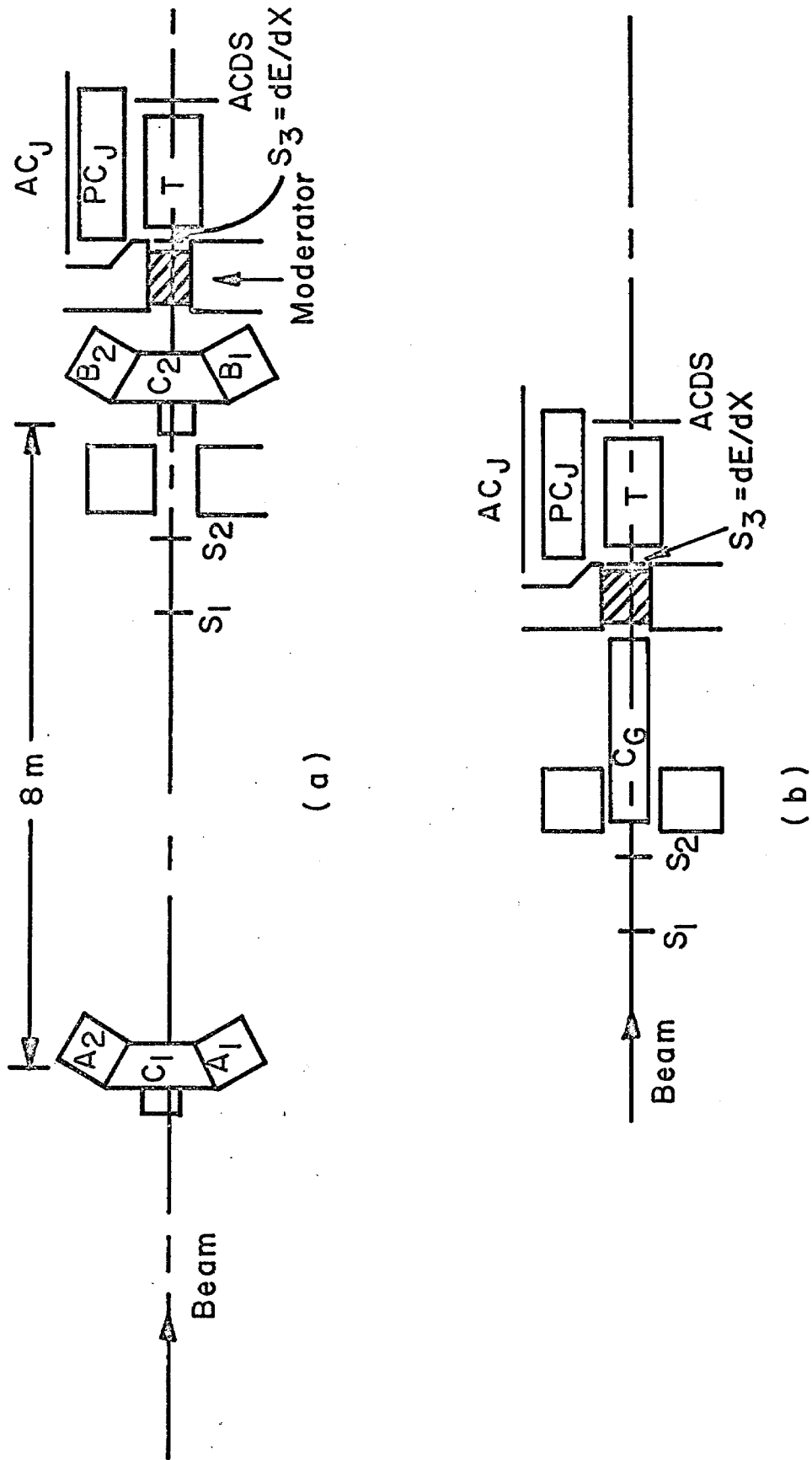
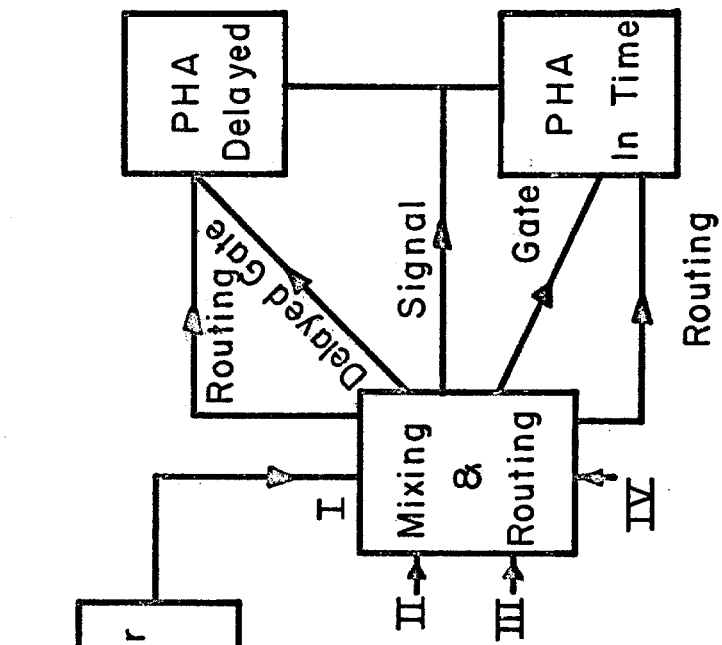


Fig. 1.

Linear Pulse Selector (LPS)



Prop. Counters 1,2 I.

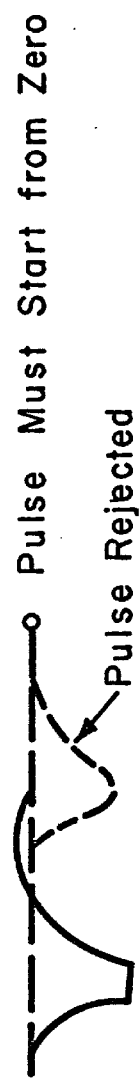
3,4 II.

5,6 III.

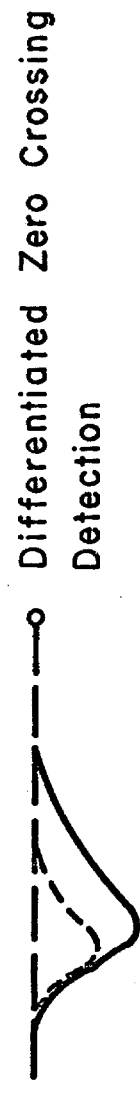
7,8 IV.

LPS Functions

1. Baseline Restoration
2. Pulse Shape Detection
- A. Baseline Detection



3. Linear Gate Shaping
4. Mixer Pileup Anti



3. Linear Gate Shaping
4. Mixer Pileup Anti

Fig. 2.

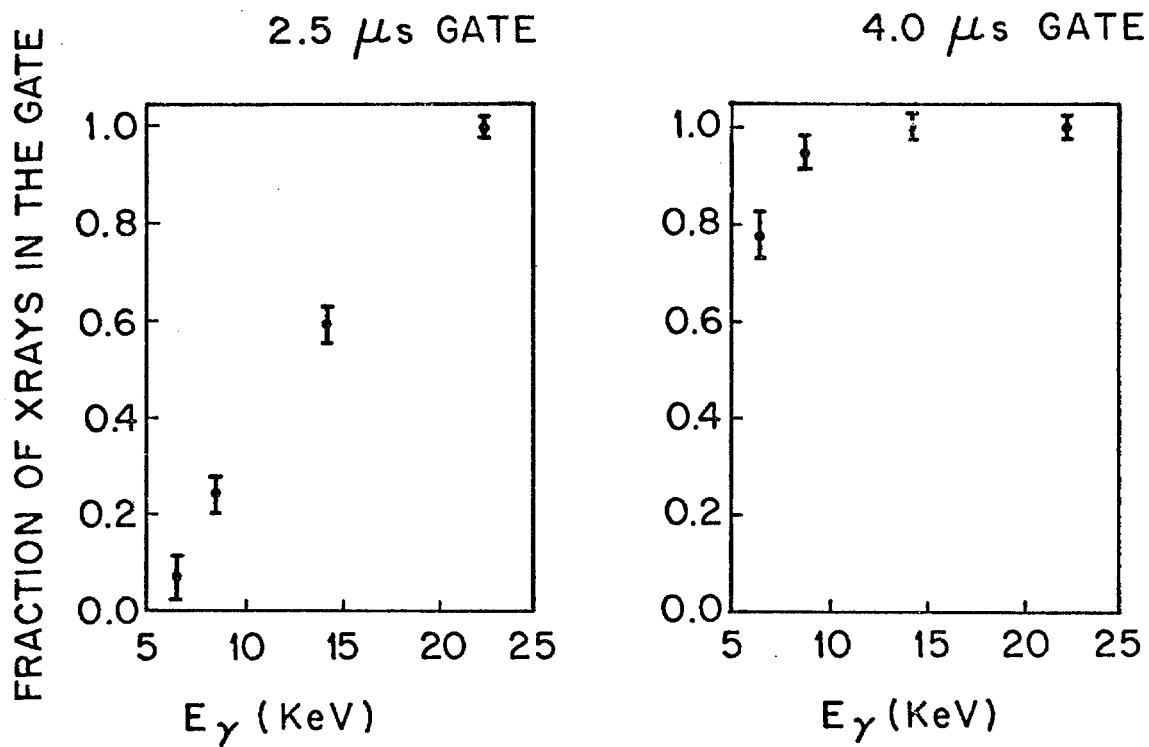


Fig. 3.

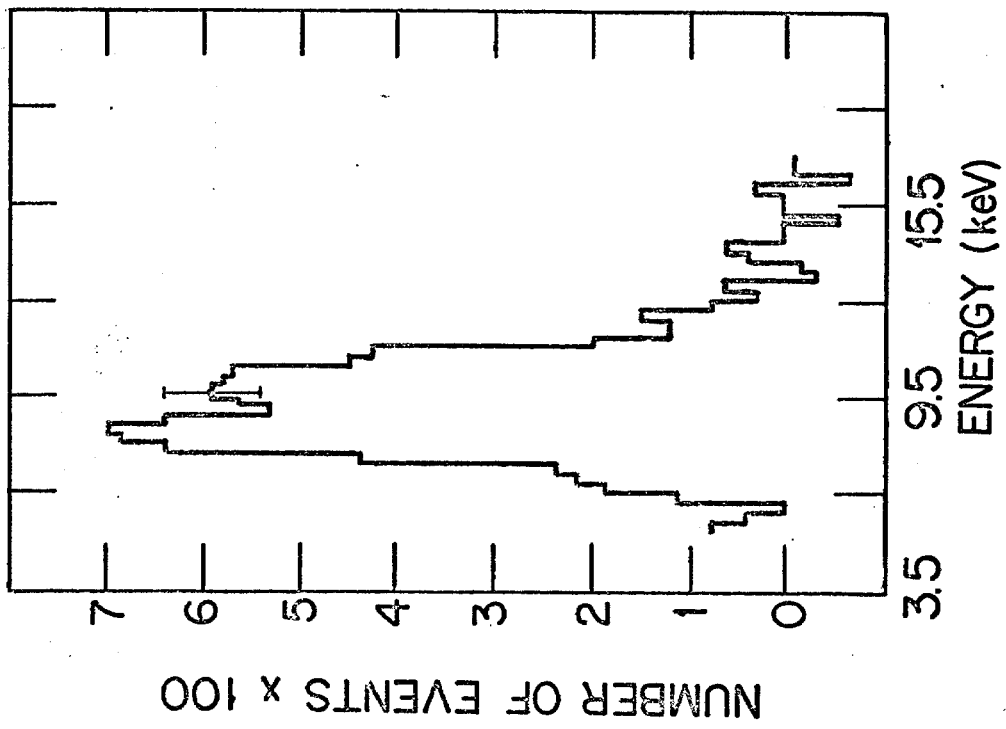
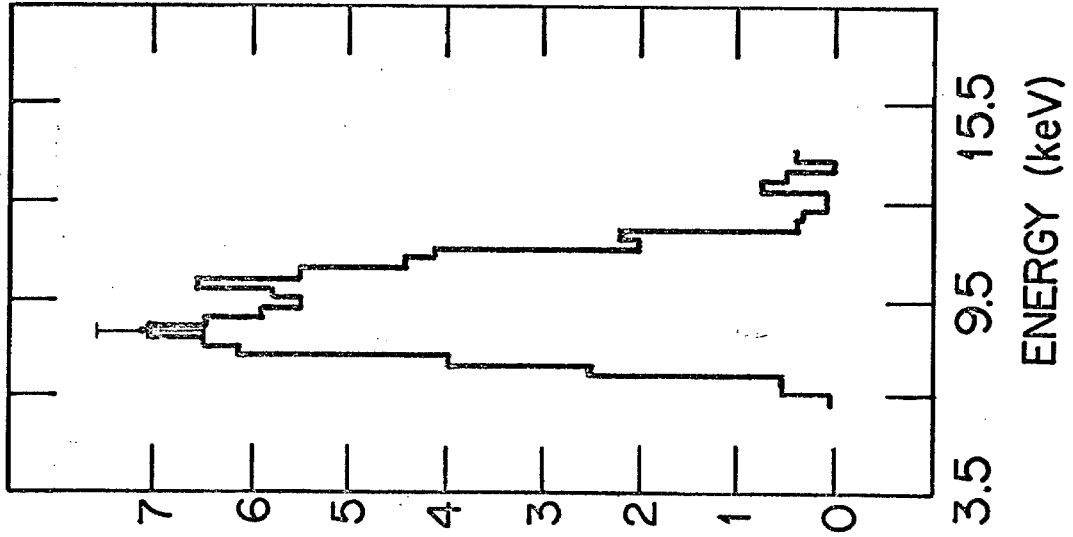


Fig. 4.

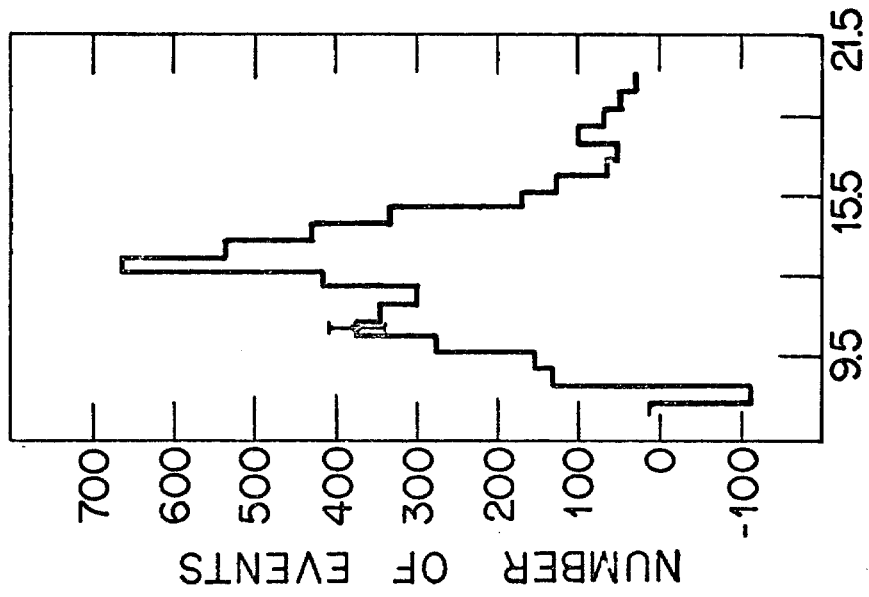


Fig. 5.

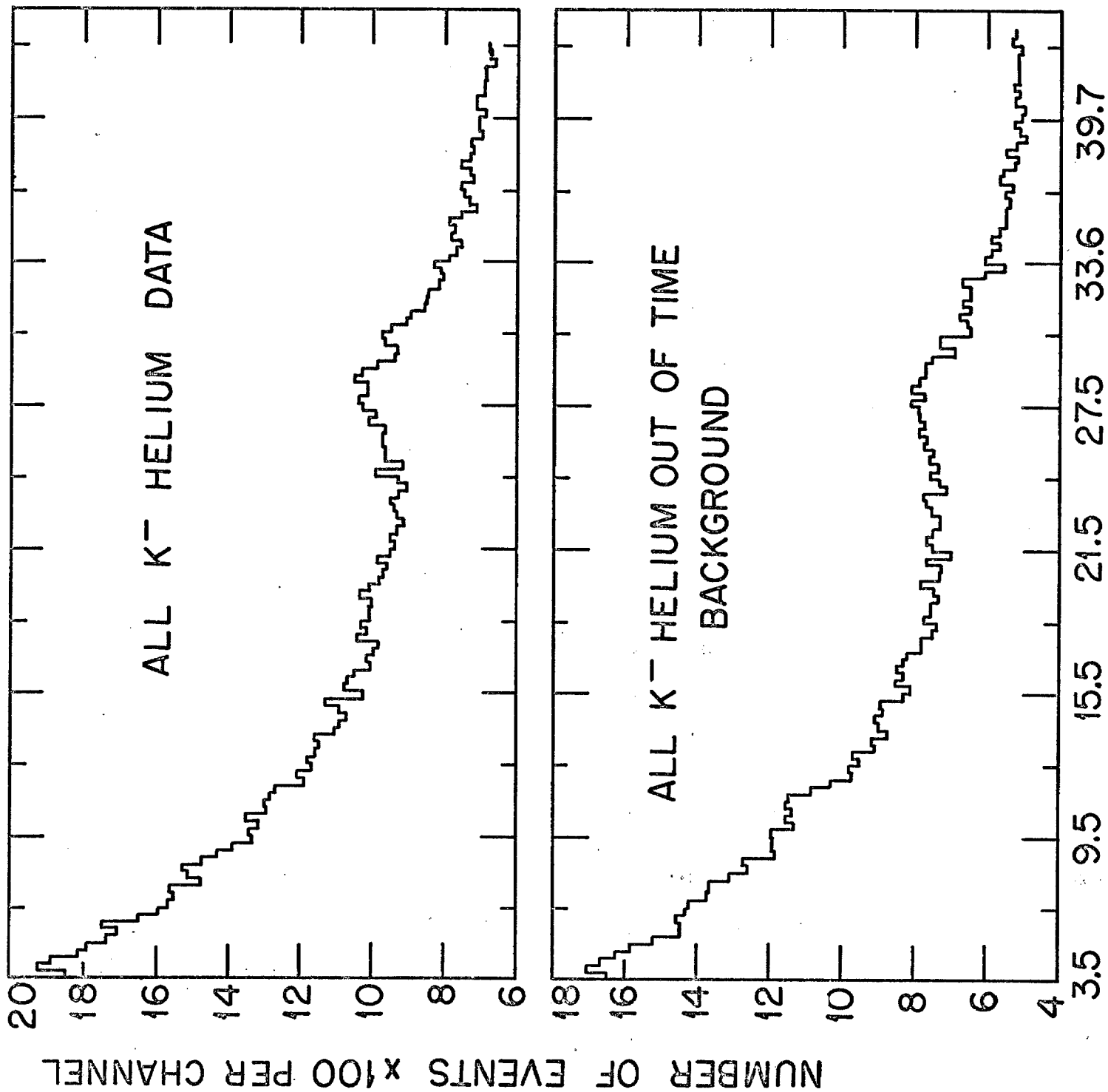


Fig. 6.

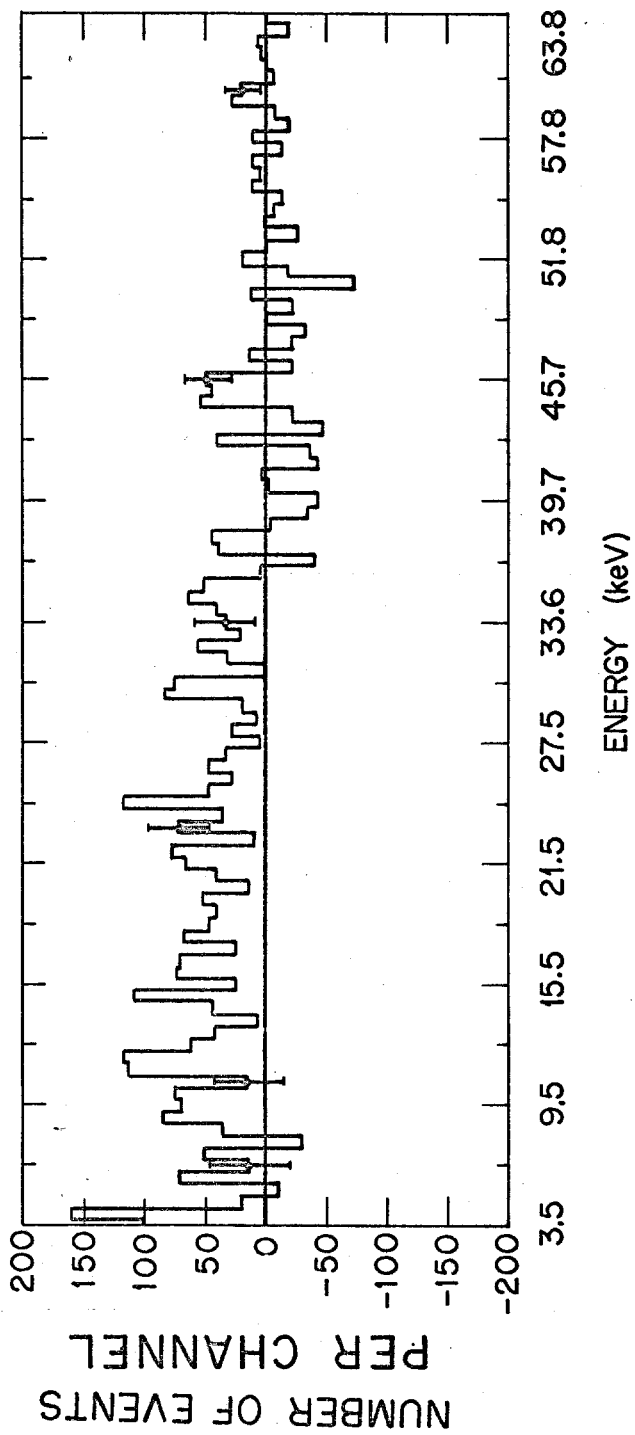


Fig. 7.

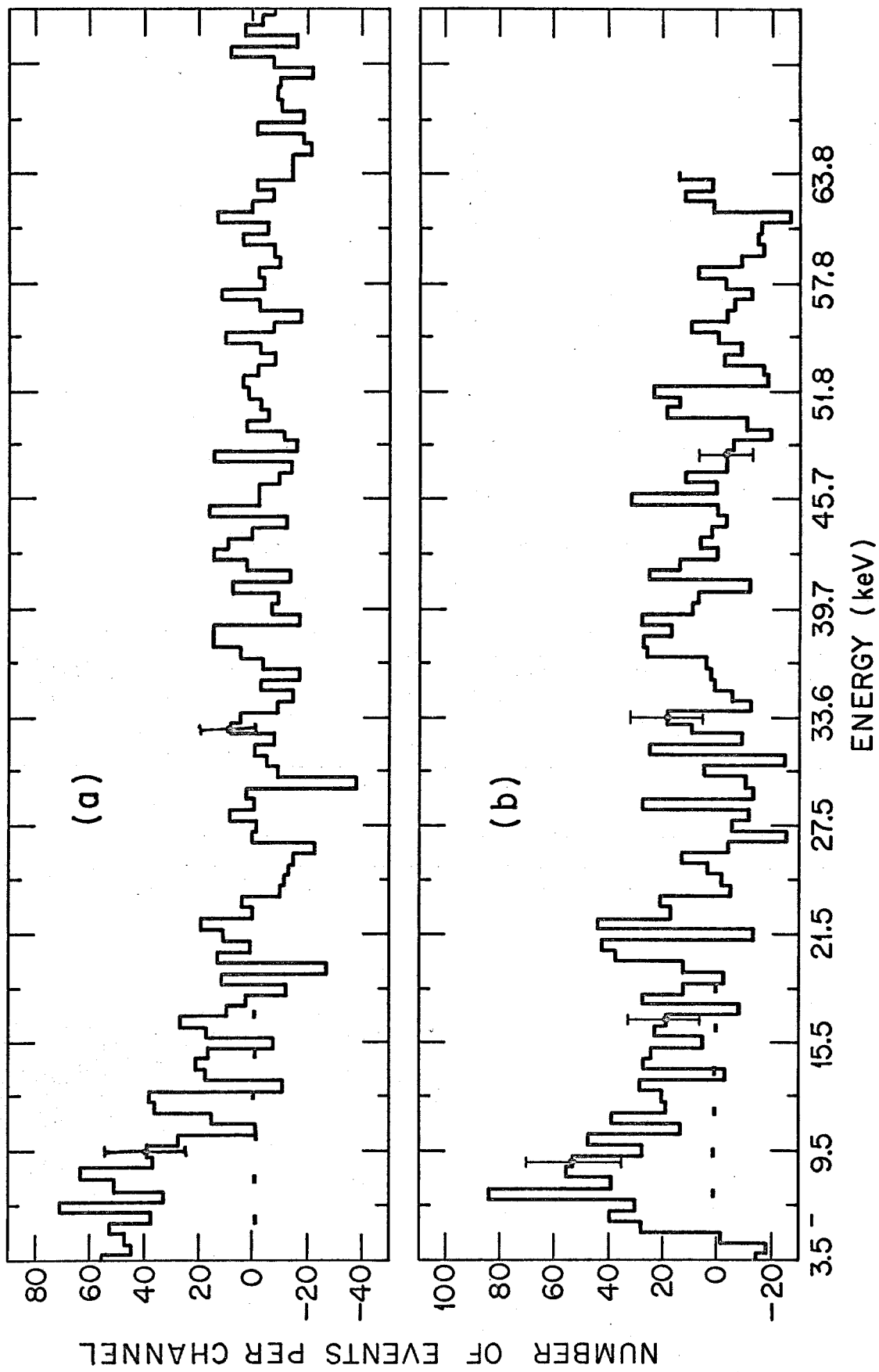


Fig. 8.

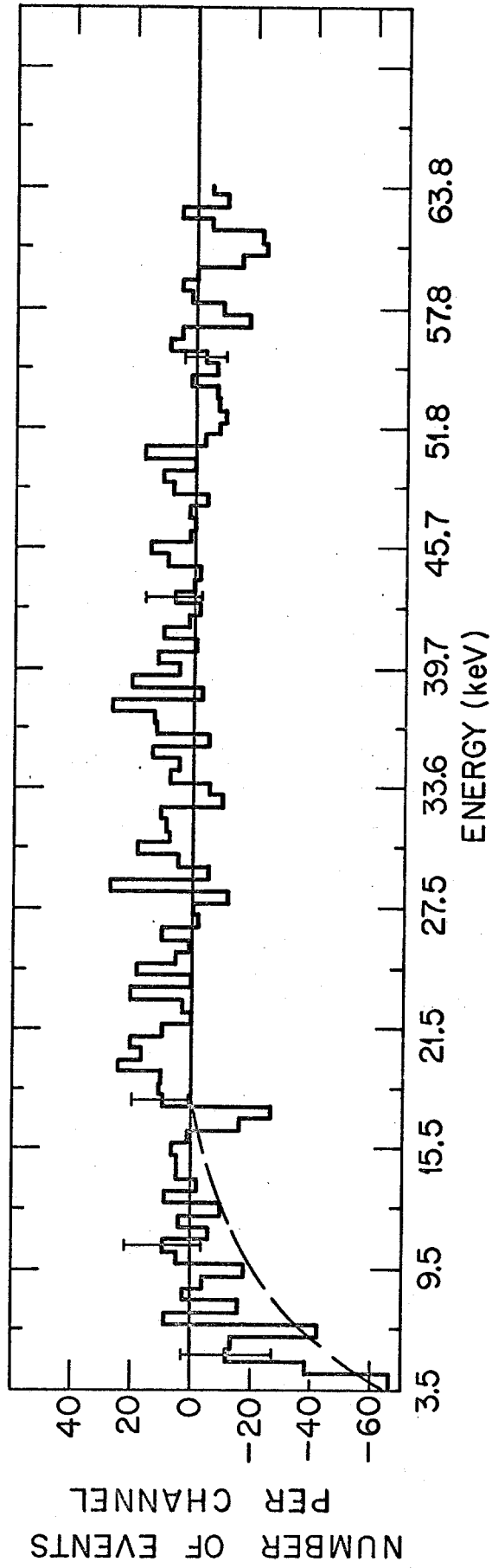


Fig. 9.

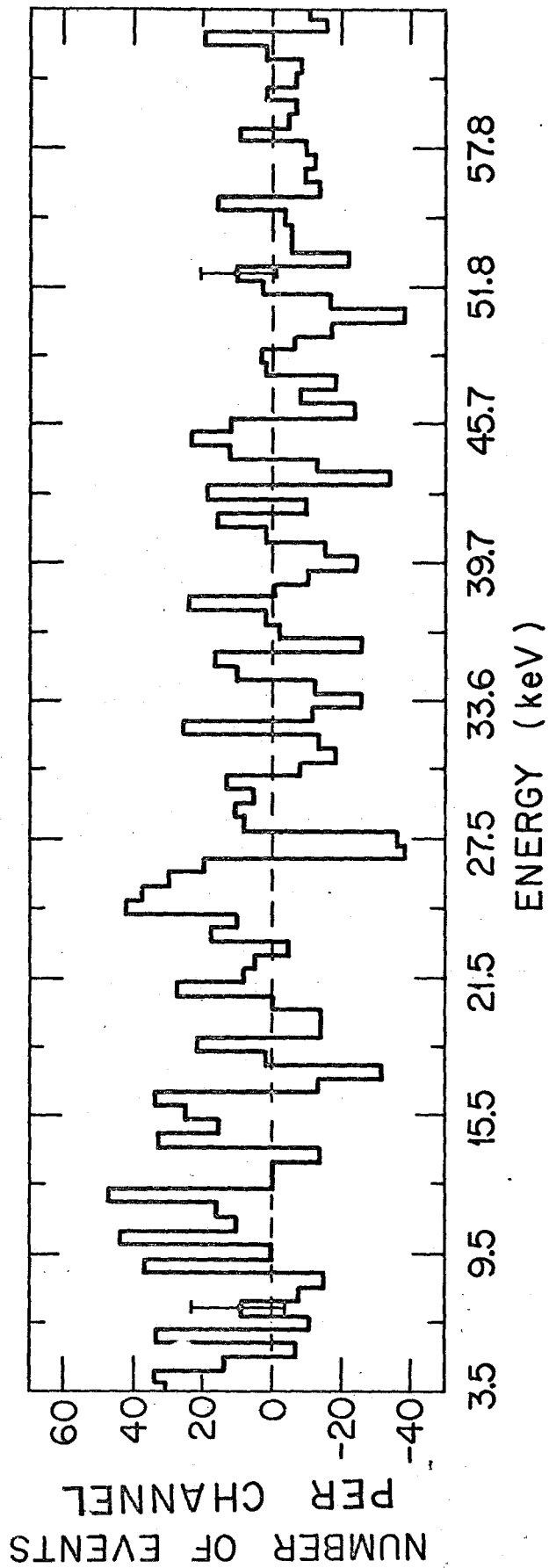


Fig. 10.

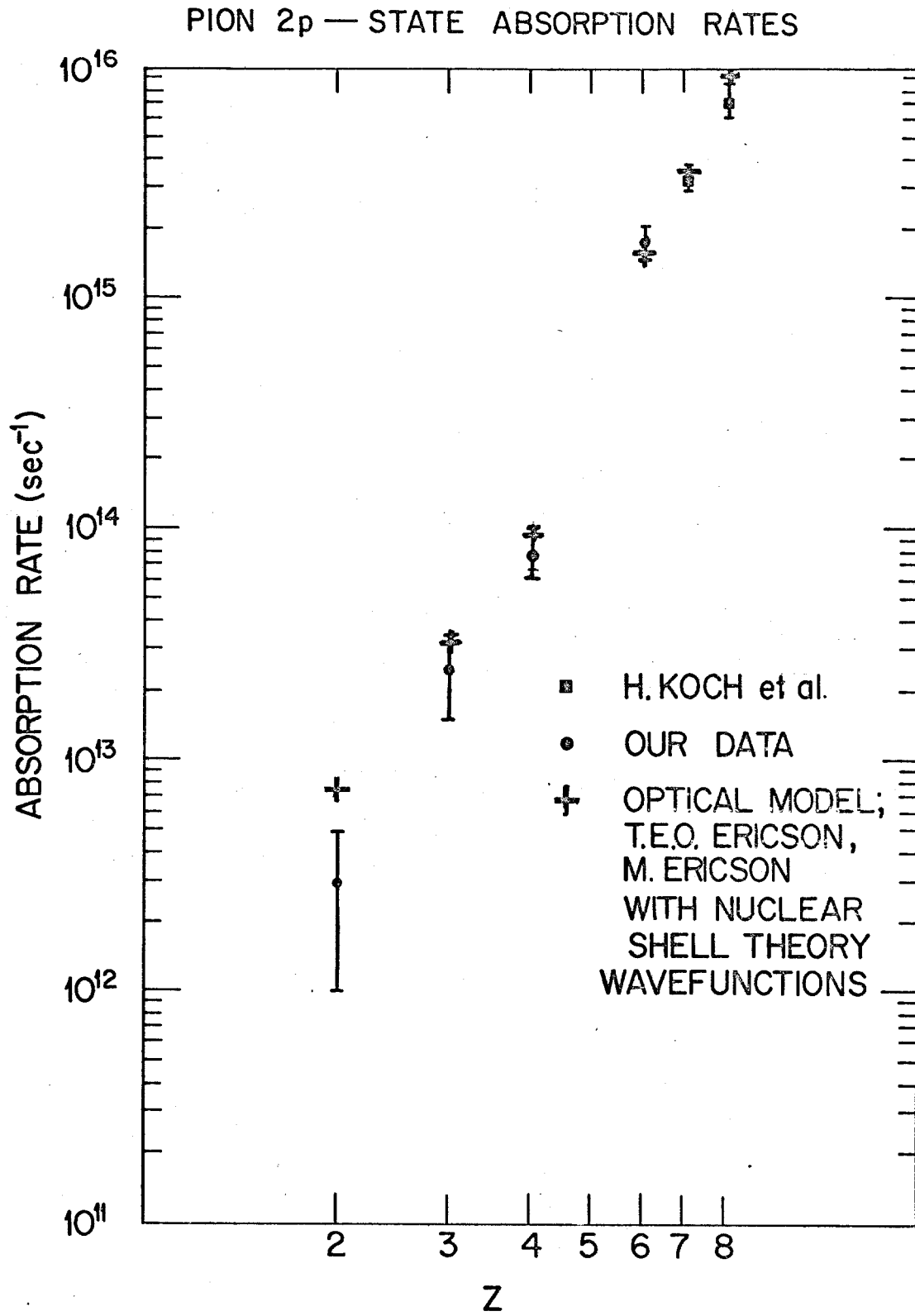


Fig. 11.

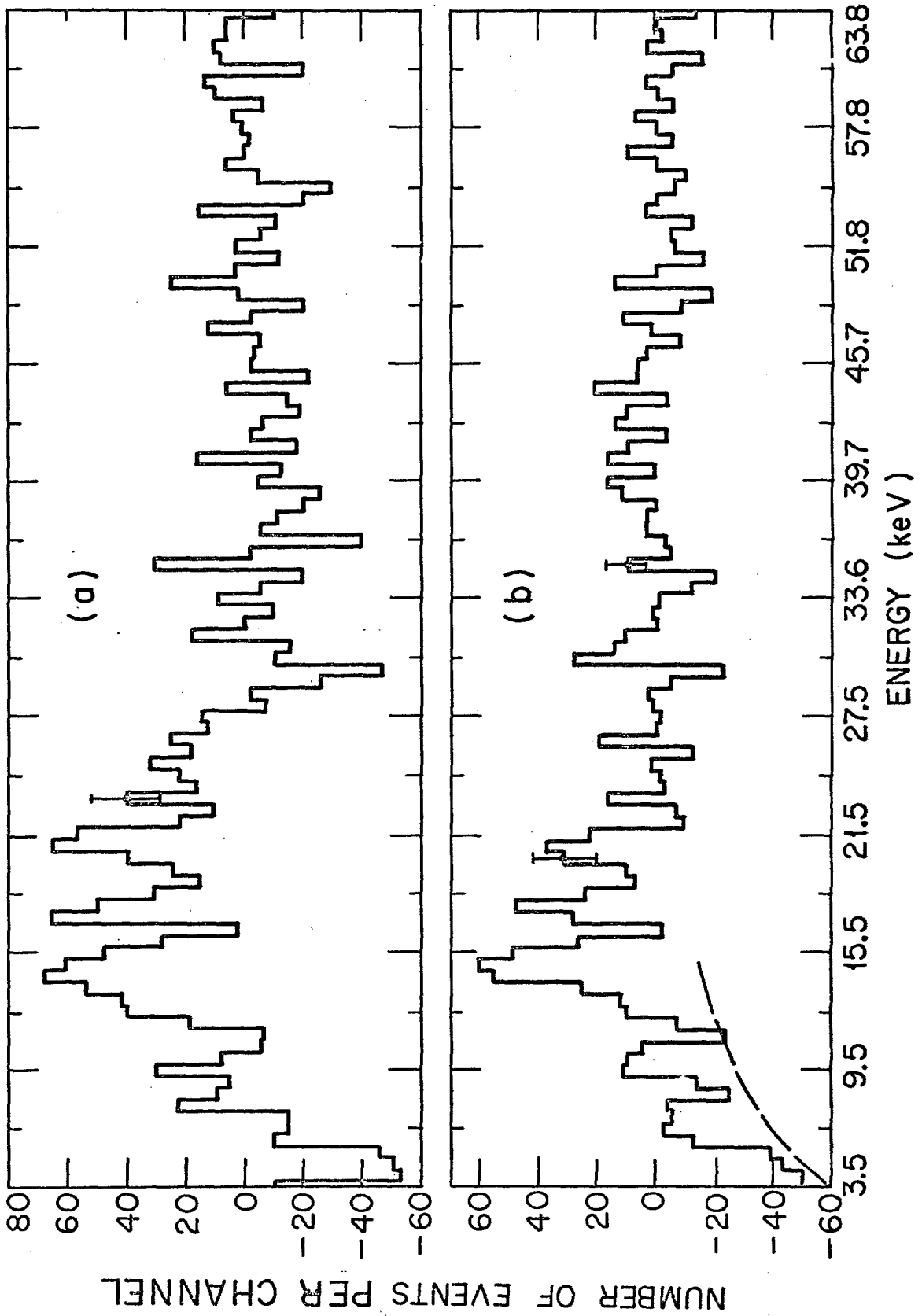


Fig. 12.

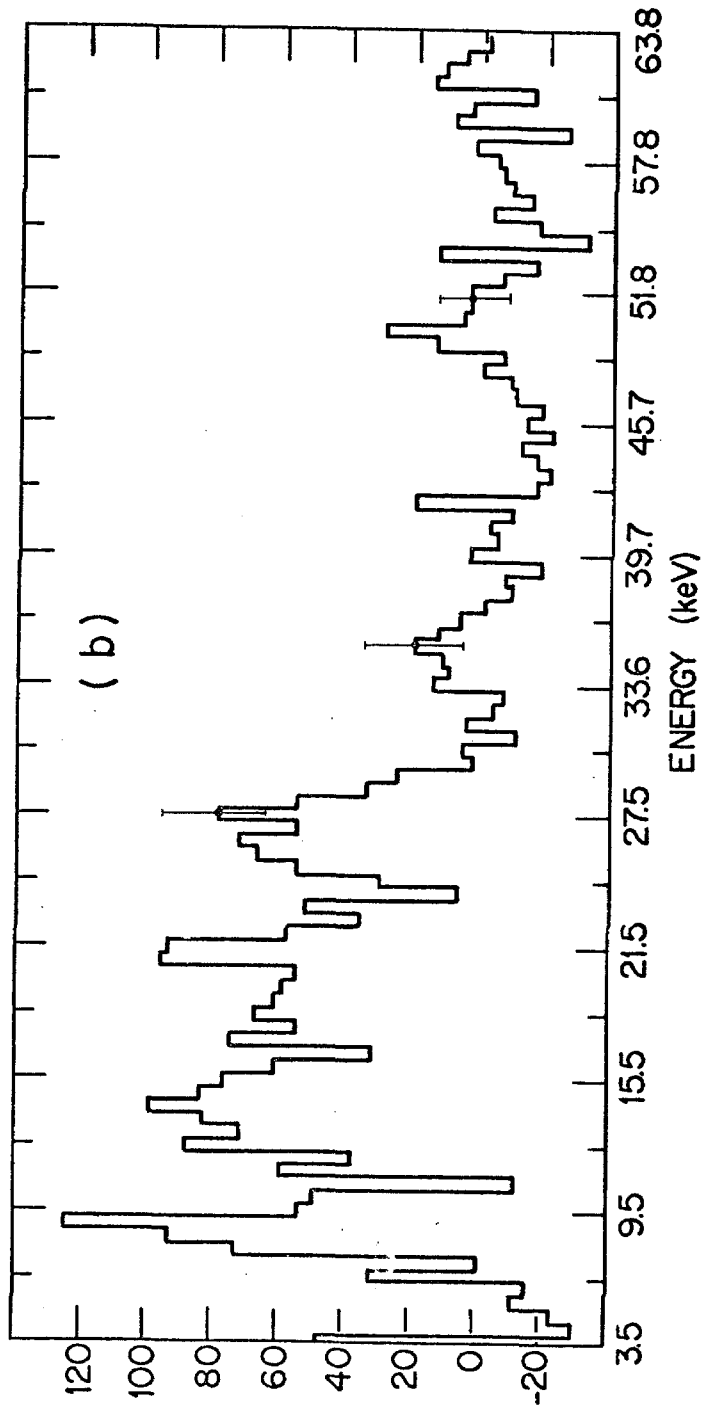
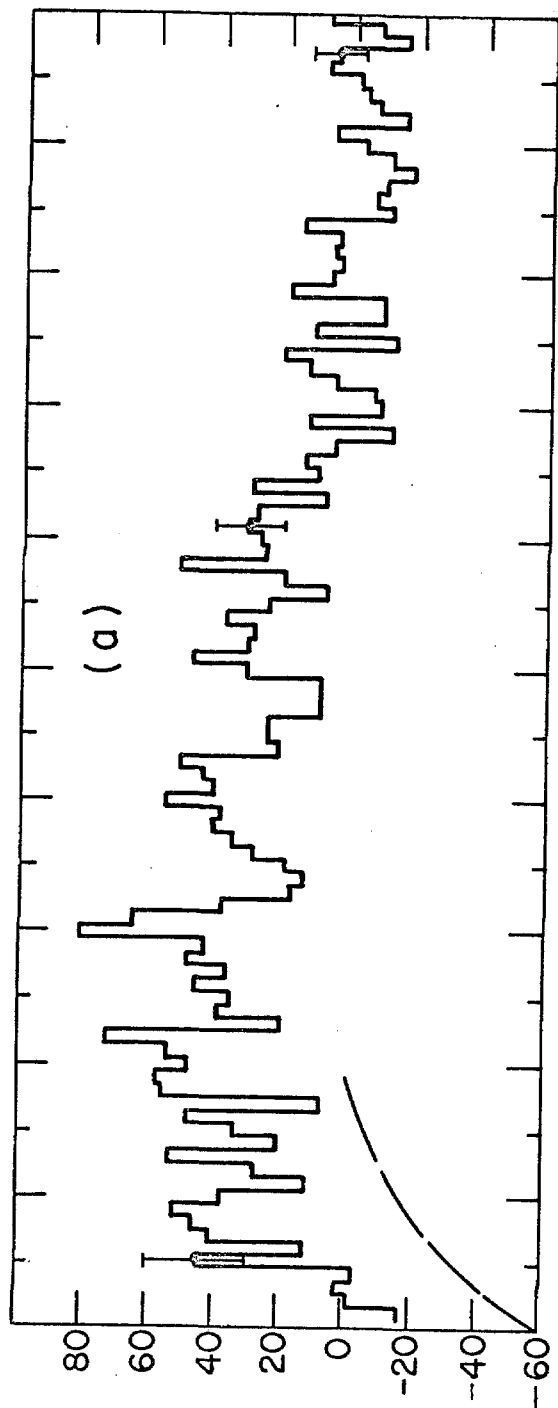


Fig. 13.

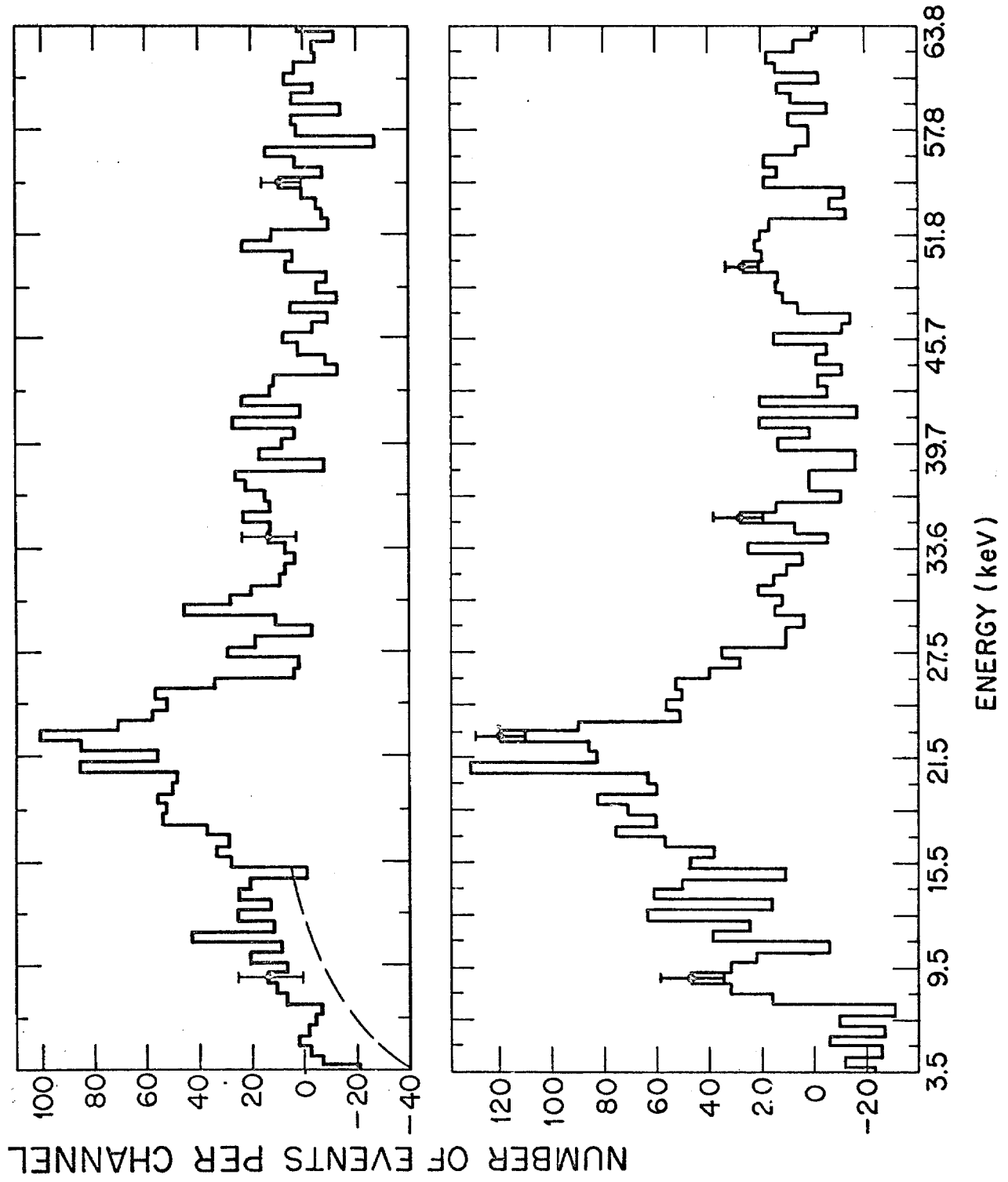
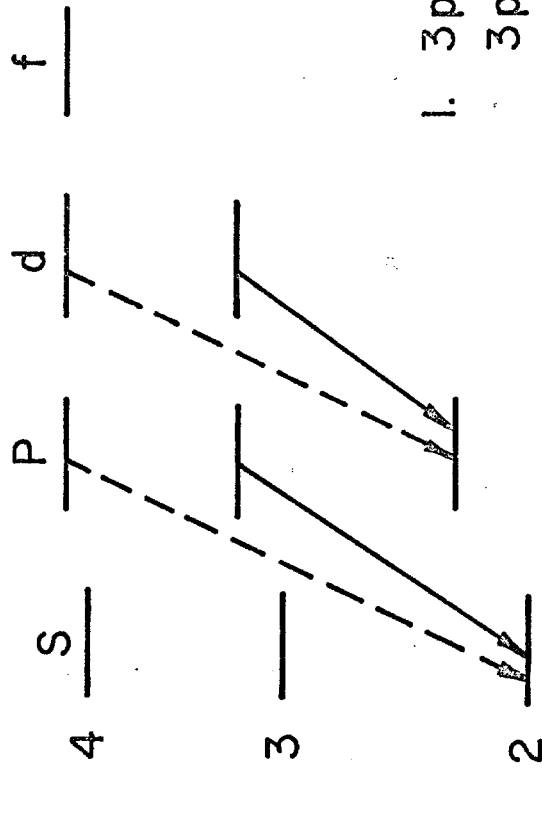


Fig. 14.

Possible Origin of L_{α}' , L_{β}' Lines from Level Shifts:



If L_{α} , L_{β} Split:

1. $3p$, $4p$ population then known.
 $3p \rightarrow 1s$, $4p \rightarrow 1s$ transition rates
 should exceed $3p \rightarrow 2s$, $4p \rightarrow 2s$
2. p absorption rates are too high.

$n = 1$ —

Fig. 15.

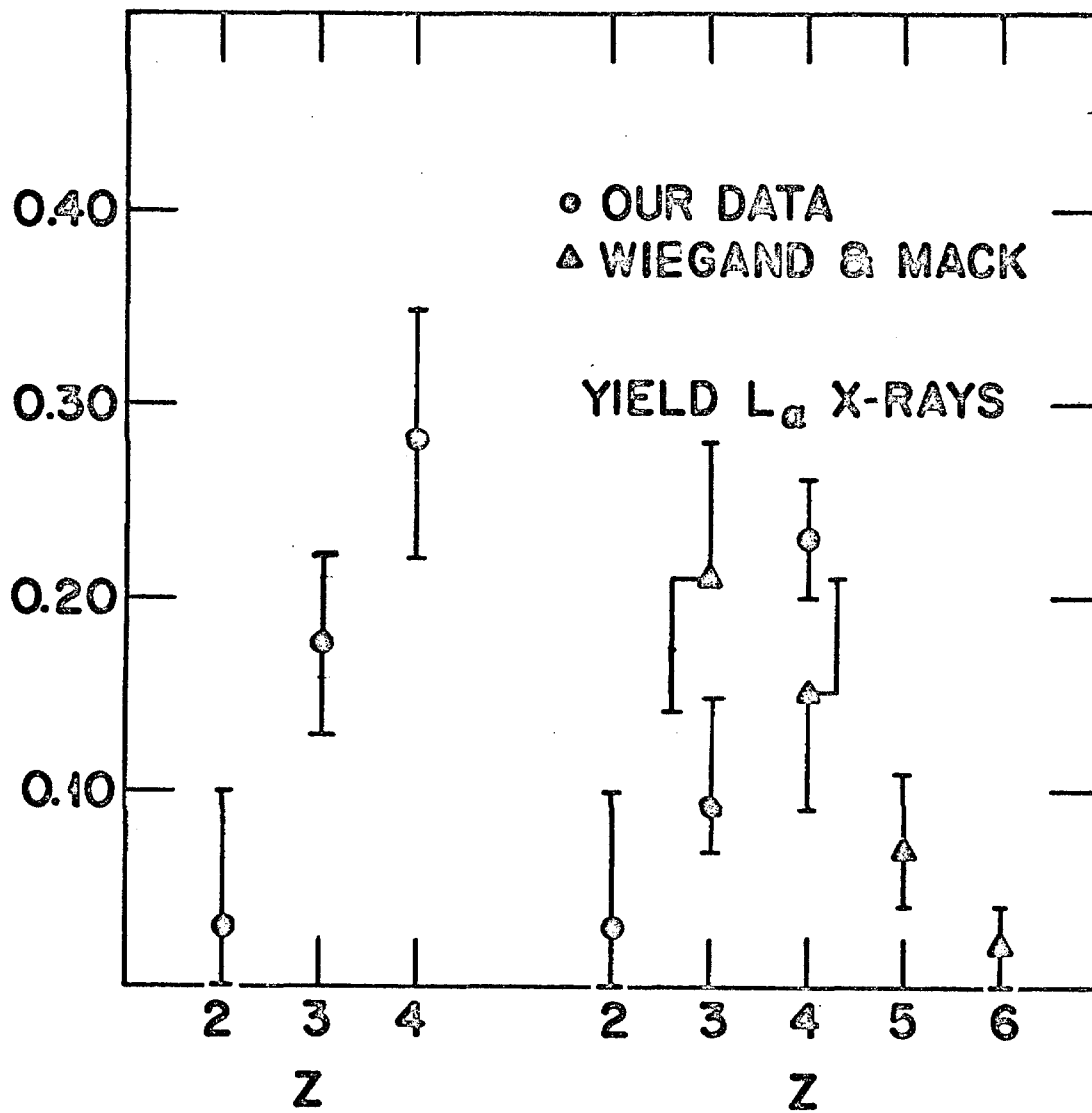


Fig. 16.

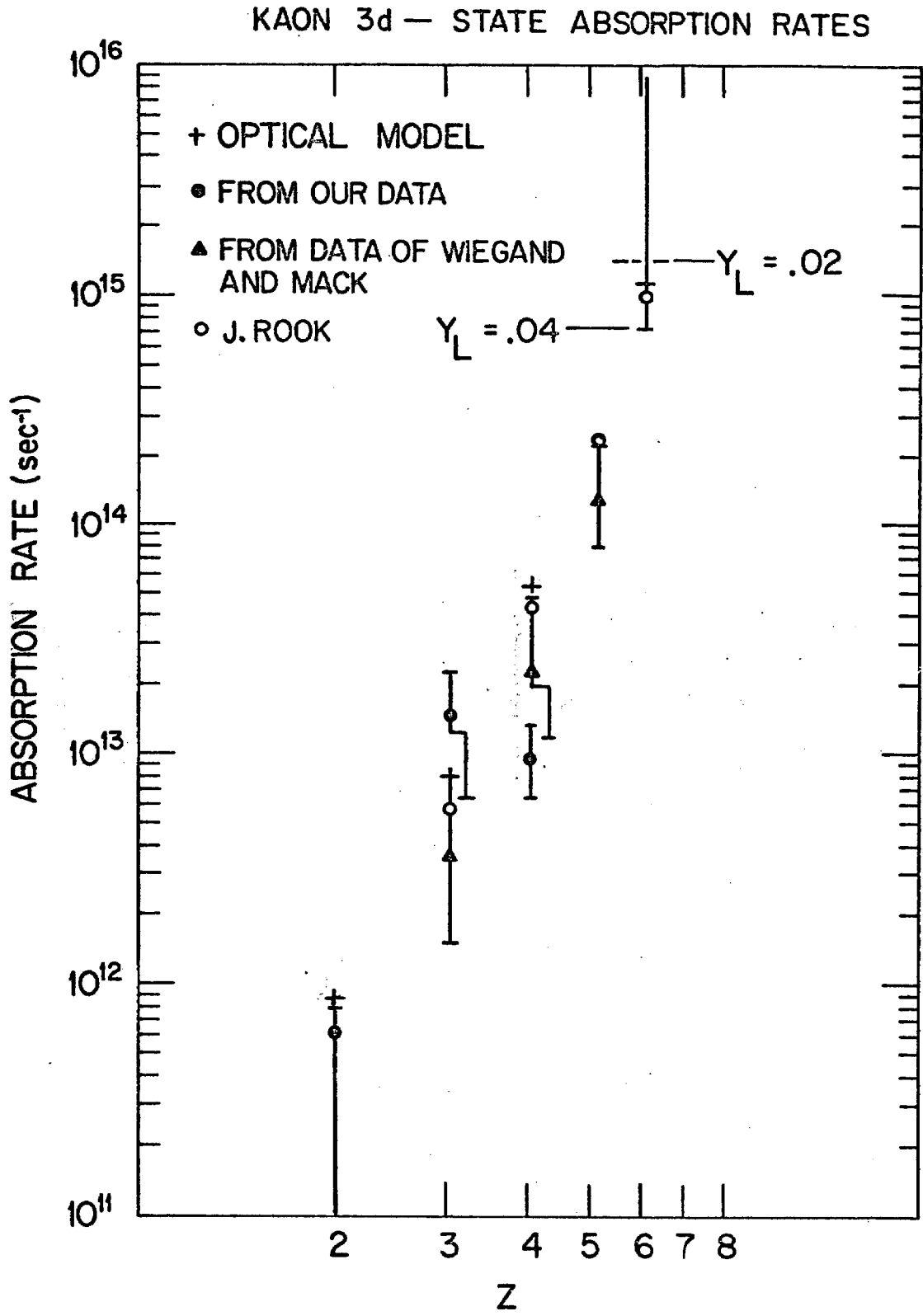


Fig. 17.